

# Effect of Coating Material on High Temperature Oxidation of Inconel 738LC Superalloy

İzmir Katip Celebi University  
Graduate School of Natural and Applied  
Sciences  
Master of Material Science and Engineering

by  
Simge AVCI  
ORCID 0000-0001-7737-3890

May, 2023

This is to certify that we have read the thesis **Effect of Coating Material on High Temperature Oxidation of Inconel 738LC Superalloy** submitted by **Simge AVCI**, and it has been judged to be successful, in scope and in quality, at the defense exam and accepted by our jury as a master's / thesis.

**APPROVED BY:**

**Advisor:** **Assoc. Prof. Dr. Onur ERTUĞRUL**  
İzmir Kâtip Çelebi University

**Committee Members:**

**Assoc. Prof. Dr. Esra DOKUMACI ALKAN**  
Dokuz Eylül University

**Assoc. Prof. Dr. Ege Anıl DİLER**  
Ege University

**Date of Defense: May 05, 2023**

# Declaration of Authorship

I, **Simge AVCI**, declare that this thesis titled **Effect of Coating Material on High Temperature Oxidation of Inconel 738LC Superalloy** and the work presented in it are my own. I confirm that:

- This work was done wholly or mainly while in candidature for the Master's / Doctoral degree at this university.
- Where any part of this thesis has previously been submitted for a degree or any other qualification at this university or any other institution, this has been clearly stated.
- Where I have consulted the published work of others, this is always clearly attributed.
- Where I have quoted from the work of others, the source is always given. This thesis is entirely my own work, with the exception of such quotations.
- I have acknowledged all major sources of assistance.
- Where the thesis is based on work done by myself jointly with others, I have made clear exactly what was done by others and what I have contributed myself.

Date: 05.05.2023

---

# Effect of Coating Material on High Temperature Oxidation of Inconel 738LC Superalloy

## Abstract

Inconel 738LC is a nickel-based superalloy commonly used in gas turbines, turbine nozzles and turbine blades. Inconel 738LC, which is frequently used in gas turbine engine components, is exposed to high temperature and high corrosion. Therefore, the high temperature resistance values and high temperature oxidation resistance of this material become critical.

In this study, the mechanical and microstructural effects of carbon in Inconel 738 alloy were investigated. The results of tensile tests at room temperature and at two different high temperatures were compared. The effects on the phase structure were evaluated by microstructure studies. For mechanical properties at 760 and 982°C, low carbon samples gave higher yield strength, tensile strength and elongation values. The reasons for these results were primarily attributed to the reduction of  $\gamma$  and  $\gamma'$  phases, thus increasing MC and M<sub>6</sub>C carbides, but also to the reduction of grain size with lower carbon content. In the continuation of the study, the resistance of Inconel 738LC alloy, known as low carbon, to high temperature oxidation with two different coating types was interpreted. The compatibility of the coating types with the main metal, Inconel 738LC, was evaluated by SEM analyzes made after the high temperature corrosion test. The effectiveness of two different coating powder alloys was evaluated comparatively by SEM analysis. In the oxidation test at 850°C, the oxygen content on the surface increased from 23% in the uncoated sample to 33-36% in the coated samples. It was observed that both coating types applied were not suitable for the working ambient temperature of Inconel 738 low carbon material. Considering the temperature-dependent behavior of the oxygen affinity of the base element in the plating alloy, it has been observed that the oxidation resistance of the chromium-based coating, known as the refractory metal, is higher.

**Keywords:** Inconel 738LC, VIM, V-IC, Carbon Level, High Temperature Corrosion, HVOF Coating

# Kaplama Malzemesinin Inconel 738LC Süperalaşımının Yüksek Sıcaklıkta Oksidasyon Davranışına Etkileri

## ÖZ

Inconel 738LC alaşımı nikel bazlı bir süperalaşımdır ve genellikle gaz türbinlerinde, türbin nozullerinde ve türbin bıçaklarında kullanılmaktadır. Gaz türbin motoru bileşenlerinde kullanımı yaygın olan Inconel 738LC çalışma ortam koşulları sebebi ile yüksek sıcaklık ile birlikte yüksek korozyona da maruz kalmaktadır. Bu sebeple, bu malzemenin yüksek sıcaklık mukavemet değeri ve yüksek sıcaklık oksidasyon direnci büyük önem taşımaktadır.

Bu çalışmada karbon elementinin Inconel 738 alaşımında mekanik ve mikroyapısal etkileri incelenmiştir. Oda sıcaklığında ve iki farklı yüksek sıcaklıktaki çekme testlerinin sonuçları karşılaştırılmıştır. Mikroyapı çalışmaları ile faz yapısına olan etkileri değerlendirilmiştir. 760 ve 982°C'de mekanik özellikler için, düşük karbonlu numuneler daha yüksek akma mukavemeti, çekme mukavemeti ve uzama değerleri vermiştir. Bu sonuçların nedenleri öncelikle  $\gamma$  ve  $\gamma'$  fazlarının azalmasına, dolayısıyla MC ve M6C karbürlerin artmasına ve ayrıca daha düşük karbon içeriği ile tane boyutunun küçülmesine bağlanmıştır. Çalışmanın devamında düşük karbonlu olarak bilinen Inconel 738LC alaşımının iki farklı kaplama türü ile yüksek sıcaklık oksidasyonuna direnci yorumlanmıştır. Kaplama türlerinin, ana metal olan Inconel 738LC ile uyumunun yüksek sıcaklık korozyon testi sonrası yapılan SEM analizleri ile değerlendirmesi yapılmıştır. SEM analizi ile iki farklı kaplama toz alaşımının etkinliği karşılaştırmalı olarak değerlendirilmiştir. 850°C'de yapılan oksidasyon testinde yüzeydeki oksijen oranı kaplanmamış numunede %23 iken, kaplanmış numunelerde %33-36'ya yükselmiştir. Uygulanan iki kaplama türünde Inconel 738 düşük karbonlu malzemesinin çalışma ortam sıcaklığına uygun bulunmadığı görülmüştür. Kaplama alaşımında bulunan baz elementin oksijen afinitesinin sıcaklığa bağlı davranışları da göz önünde bulundurulduğunda refrakter metal olarak

bilinen krom bazlı kaplamanın, oksidasyon direncinin daha yüksek olduđu görölmüştür.

**Anahtar Kelimeler:** Inconel 738LC, VIM, V-IC, Karbon Seviyesi, Yüksek Sıcaklık Korozyonu, HVOF Kaplama

*To my dear FAMILY and my dear fiance Ozan DEMİRKAYA for their unwavering support for this thesis.*

# Acknowledgment

I would like to thank Assoc. Prof. Dr. Onur Ertuğrul for his guidance and assistance. I would like to thank Rabia Günay and Cemre Tıǒlı from Tusaş Engine Industry, İsmail Demirkaya and Alp Demirkapu from Varzene Metal for their support throughout the thesis.



# Table of Contents

Declaration of Authorship .....	ii
Abstract .....	iii
Öz .....	iv
Acknowledgment .....	vi
List of Figures .....	x
List of Tables.....	xi
List of Abbreviations.....	xii
List of Symbols .....	xiii
<b>1 Introduction .....</b>	<b>1</b>
1.1 Aim and Objective of the Thesis .....	1
1.2 Theoretical Background.....	2
1.2.1 History of Superalloys .....	2
1.2.2 Properties of Superalloys.....	3
1.2.3 Classification of Superalloys .....	6
1.2.3.1 Iron-based Superalloys .....	6
1.2.3.2 Cobalt-based Superalloys .....	8
1.2.3.3 Nickel-based Superalloys .....	8
1.2.4 Inconel 738 and Inconel 738LC Alloys.....	10
1.2.5 Manufacturing Methods of Superalloys .....	13
1.2.5.1 Vacuum Induction Melting (VIM).....	14
1.2.5.2 Investment Casting .....	15
1.2.5.3 Heat Treatment .....	16

1.2.6	Coatings for Superalloys .....	16
1.2.7	High Temperature Oxidation (Hot Corrosion) .....	20
1.2.8	Literature Overview .....	22
<b>2</b>	<b>Materials and Methods .....</b>	<b>24</b>
2.1	Material and Production Process .....	24
2.2	Heat Treatment Process .....	27
2.3	HVOF Thermal Spray Coating .....	27
2.4	Characterization Studies .....	30
2.4.1	Mechanical Testing .....	30
2.4.2	Microstructural Analysis .....	32
2.4.3	High Temperature Oxidation Test .....	32
2.4.4	Scanning Electron Microscopy (SEM) Analysis .....	33
<b>3</b>	<b>Results and Discussion .....</b>	<b>36</b>
3.1	Mechanical Test Results .....	36
3.1.1	Stress Rupture Test Results .....	36
3.1.2	High Temperature Tensile Test Results .....	38
3.1.3	Room Temperature Tensile Test Results .....	44
3.2	Microstructural Study Results .....	48
3.3	Oxidation Test Results .....	50
3.3.1	Weight Changes .....	50
3.3.2	SEM Analyzes .....	52
<b>4</b>	<b>Conclusion .....</b>	<b>71</b>
	<b>References .....</b>	<b>74</b>
	<b>Curriculum Vitae .....</b>	<b>79</b>

# List of Figures

Figure 1.1	Gas turbine engine using nickel-based superalloys effectively .....	9
Figure 1.2	Chromium containing nickel-based superalloys and microstructure evaluation .....	10
Figure 1.3	Processing routes for superalloys .....	14
Figure 1.4	Steps in investment casting process.....	16
Figure 1.5	HVOF process .....	20
Figure 1.6	For Inconel 718 material a) before high temperature oxidation test, b) isothermal after 18 hours, c) after 6 hours (1st cycle), d) after 12 hours (2nd cycle) and e) after 18 hours (3rd cycle) macro images.....	21
Figure 2.1	Ingots for investment casting .....	26
Figure 2.2	Blank sample produced by vacuum investment casting.....	26
Figure 2.3	Sandblasting machine.....	28
Figure 2.4	Sample surfaces after the aluminum oxide sandblasting .....	29
Figure 2.5	HVOF process .....	29
Figure 2.6	Tensile test samples.....	31
Figure 2.7	High-temperature tensile testing device.....	31
Figure 2.8	Electric resistance heat treatment furnace.....	32
Figure 2.9	Placement of samples in the furnace .....	33
Figure 2.10	Scanning electron microscopy (SEM) .....	34
Figure 2.11	SEM samples undergone to oxidation tests (a) at 850 °C, (b) at 1000°C. ....	35
Figure 3.1	Comparative chart for stress rupture test results.....	38
Figure 3.2	Comparative chart for stress rupture test elongation results.....	38
Figure 3.3	Comparison chart for 760°C high temperature ultimate tensile strength results .....	41
Figure 3.4	Comparison chart for 760°C high temperature yield strength results ....	41
Figure 3.5	Comparison chart for 760°C high temperature elongation results .....	42
Figure 3.6	Comparison chart for 760°C high temperature reduction area results ...	42
Figure 3.7	Comparison chart for 982°C high temperature ultimate tensile	

strength results .....	43
Figure 3.8 Comparison chart for 982°C high temperature yield strength results ....	43
Figure 3.9 Comparison chart for 982°C high temperature elongation results .....	44
Figure 3.10 Comparison chart for 982°C high temperature reduction area results ...	44
Figure 3.11 Comparison chart for room temperature ultimate tensile strength results .....	46
Figure 3.12 Comparison chart for room temperature yield strength results.....	47
Figure 3.13 Comparison chart for room temperature elongation results.....	47
Figure 3.14 Comparison chart for room temperature reduction area results.....	48
Figure 3.15 Microstructure images of IN738 sample.....	48
Figure 3.16 Microstructure images of IN738LC sample.....	49
Figure 3.17 Uncoated sample images after 4 cycles of oxidation test at 850°C .....	53
Figure 3.18 Selected area 2.....	53
Figure 3.19 EDS spot 1.....	54
Figure 3.20 Selected area 3.....	55
Figure 3.21 (WC-12Co)- 33(Cr <sub>2</sub> C <sub>3</sub> -20NiCr) coated sample images after 4 cycles of oxidation test at 850°C .....	56
Figure 3.22 Selected area 2.....	57
Figure 3.23 Selected area 3.....	58
Figure 3.24 EDS spot 1.....	59
Figure 3.25 Cr <sub>2</sub> C <sub>3</sub> -20NiCr coated sample images after 4 cycles of oxidation test at 850°C.....	60
Figure 3.26 EDS spot 1.....	60
Figure 3.27 Selected area 2.....	61
Figure 3.28 EDS spot 2 .....	62
Figure 3.29 Selected area 6.....	62
Figure 3.30 Uncoated sample images after 4 cycles of oxidation test at 1000°C.....	63
Figure 3.31 Selected area 2 .....	64
Figure 3.32 EDS spot 3.....	65
Figure 3.33 (WC-12Co)- 33(Cr <sub>2</sub> C <sub>3</sub> -20NiCr) coated sample images after 4 cycles of oxidation test at 1000°C .....	66
Figure 3.34 Selected area 3.....	66
Figure 3.35 EDS spot 2.....	67

Figure 3.36 Cr <sub>2</sub> C <sub>3</sub> -20NiCr coated sample images after 4 cycles of oxidation test at 1000°C.....	68
Figure 3.37 Selected area 2.....	68
Figure 3.38 Selected area 7.....	69
Figure 3.39 EDS spot 1 .....	70

# List of Tables

Table 1.1	Effect of elements on superalloys .....	5
Table 1.2	Major phase types formed in super alloys.....	7
Table 1.3	Chemical compositions of alloy Inconel 738.....	11
Table 1.4	Relationship between coating functions and coating material characteristics .....	17
Table 2.1	Chemical composition of the produced Inconel 738 ingot (0.19% C)....	25
Table 2.2	Chemical composition of the produced Inconel 738LC ingot (0.13% C).....	25
Table 2.3	Solution and aging heat treatments parameters.....	27
Table 3.1	Stress rupture test results of Inconel 738 (0.19% C) samples.....	37
Table 3.2	Stress rupture test results of Inconel 738 (0.13% C) samples.....	37
Table 3.3	High temperature tensile test results of Inconel 738 (0.19% C) samples. ....	40
Table 3.4	High temperature tensile test results of Inconel 738 (0.13% C) samples. ....	40
Table 3.5	Room temperature tensile test results of Inconel 738 (0.19% C) samples. ....	46
Table 3.6	Room temperature tensile test results of Inconel 738 (0.13% C) samples. ....	46
Table 3.7	Macro grain sizes observed on sample surfaces.....	50
Table 3.8	Oxidation resistance test at 850°C and 1000°C temperatures weight changes due to heat treatment steppes.....	51
Table 3.9	eZAF smart quant results of area 2 .....	54
Table 3.10	eZAF smart quant results of EDS spot 1.....	55
Table 3.11	eZAF smart quant results of area 3 .....	56
Table 3.12	eZAF smart quant results of area 2 .....	57
Table 3.13	eZAF smart quant results of area 3 .....	58
Table 3.14	eZAF smart quant results of EDS spot 1.....	59
Table 3.15	eZAF smart quant results of EDS spot 1.....	61
Table 3.16	eZAF smart quant results of area 1 .....	61
Table 3.17	eZAF smart quant results of EDS spot 2.....	62

Table 3.18 eZAF smart quant results of area 6 .....	63
Table 3.19 eZAF smart quant results of area 2 .....	64
Table 3.20 eZAF smart quant results of EDS spot 3.....	65
Table 3.21 eZAF smart quant results of area 3 .....	67
Table 3.22 eZAF smart quant results of EDS spot 2.....	67
Table 3.23 eZAF smart quant results of area 2 .....	69
Table 3.24 eZAF smart quant results of area 7 .....	69
Table 3.25 eZAF smart quant results of EDS spot 1.....	70

# List of Abbreviations

4D	Four Direction
Al	Aluminum
AOD	Argon Oxygen Decarburization
B	Boron
C	Carbon
Co	Cobalt
Cr	Chromium
CVD	Chemical Vapor Deposition
EAF	Electric Arc Furnace
FCC	Face Centered Cubic
Fe	Iron
GFQ	Gas Fan Quench
h	Hour
HTHC	High-Temperature Hot Corrosion
İKÇÜ	İzmir Kâtip Celebi University
kg	Kilogram
La	Lanthanum
LC	Low Carbon
LTHC	Low Temperature Hot Corrosion
MC	Carbide compound of 4th and 5th group metal (such as M:Ta, Ti, Hf) elements
mm	Millimeter
MPa	Mega Pascal
MPD	Melting Point-Reducing
Ni	Nickel
SEM	Scanning Electron Microscopy



Ta	Tantalum
Ti	Titanium
TLP	Transient Liquid Phase
VIM	Vacuum Induction Melting
W	Tungsten
Y	Yttrium
CN	Carbonitride
Nb	Niobium
Hf	Hafnium
Zr	Zirconium
UTS	Ultimate Tensile Strength
YS	Yield Strength
RA	Reduction of Area Percentage

# List of Symbols

$\gamma'$	Gamma
$\eta$	Eta
$\sigma$	Sigma
$^{\circ}\text{C}$	Celsius
%	Percent
kg	Mass
$\emptyset$	Diameter
$\mu\text{m}$	micrometer

# Chapter 1

## Introduction

### 1.1 Aim and Objective of the Thesis

The element carbon has various effects in alloying for steels and also superalloys. In this study, carbon-dependent variations of mechanical and microstructural properties of Inconel 738 alloy, known as a nickel-based superalloy, were investigated. Nickel is not a carbide-forming element. It has been mentioned in various studies that the element carbon has a negative or forceful effect on the mechanical and microstructural properties of an alloy. The element carbon reacts with other elements in the alloy to form carbides. It is known that the carbon element also has an effect on the high temperature resistance of nickel-based superalloys. As known the degradation due to corrosion started from the points where these carbide structures are located. In order to observe and interpret these effects in the best way, tensile tests and stress rupture tests are applied to Inconel 738 and Inconel 738LC samples produced within the scope of the study at room temperature and two different high temperatures. The carbide structures in the samples are interpreted using a scanning electron microscope. In this study, it was aimed to determine the effects of carbon on Inconel 738 alloy by examining the carbide class and its effect on the alloy.

The coating process is applied to prevent corrosion of the surface with high temperature and the growth of the oxide layer. Coating functions and coating material characteristics are important for nickel-based superalloys, which are used in high temperature working environments. Coating selection is critical because of its oxidation/corrosion behavior. In the second stage of this study, it was aimed to investigate the compatibility of coating types with Inconel 738LC alloy and the

effect of high temperature oxidation test on corrosion properties at high temperature by applying two different coatings to Inconel 738LC alloy, which primarily used in aerospace industry.

## 1.2 Theoretical Background

### 1.2.1 History of Superalloys

In 1872, George Bailey Brayton, by describing the Brayton cycle, stated that in a system operating with a temperature index, the efficiency increases as the inlet temperature increases. This development helped invent the steam turbine in the 19th century. After this discovery, the use of gas turbines started in the early 1900s [1]. It has been observed that the development of high-temperature applications and technologies related to this transformation can only be possible with materials designed for high-temperature environments. For many years in the industry, austenitic stainless steels have been preferred in operations involving high temperature working environments. However, titanium alloys have been preferred instead of austenitic stainless steels, since the strength of these steels at high temperatures is not at the desired performance. However, the problem of oxidation of titanium alloys also prevented the desired performance in operations. In the following years, as the alloying process developed, superalloys began to be produced and used in components. The development of superalloys and their observed strength with use has led to their use in gas turbine engines.

The word "superalloy" was first used in the mid-1940s to describe high-temperature alloys that can only be used in high-temperature application areas and retain their strength and toughness in these environmental conditions. The first applications were gas turbine engines developed for jet aircraft, which are aircraft carriers. Over time, it has continued its development through hundreds of scientific studies and trademarks [2].

The development of superalloys is based on both diversification of chemical compositions and innovations in process processes. Superalloys increase high temperature resistance by solid solution reinforcement method. The most important

of these strengthening mechanisms is precipitation hardening, which produces secondary phase precipitates such as  $\gamma'$  and carbides. Some elements, such as aluminum and chromium, impart oxidation and corrosion resistance to superalloys [3].

## 1.2.2 Properties of Superalloys

In operating conditions at very high temperatures; V-A group (vanadium, niobium, tantalum) and VI-A group (chromium, molybdenum, tungsten) metals are needed as refractory material as well as ceramics. The oxidation resistance of metals used as refractory materials is very low, so these materials are mostly used in areas that are not subject to oxidation. Ceramic materials, on the other hand, do not have sufficient toughness for many structural applications. Inadequate material technology in applications and limitations in current technology have made the use of superalloy materials inevitable.

Superalloys; are metallic materials that are generally developed from VIII-A group elements for use at high temperatures. Surface stability and relatively high mechanical stress properties are required for materials to be used at high temperatures (Bradley, 1979). Superalloys are alloys designed for use in the production of aircraft turbine engines and super turbochargers, which require high strength and best performance at high temperatures, and are still under development (Betteridge et al., 1974). These alloys are generally produced by combining iron, nickel, cobalt and chromium in different combinations. In addition, low rates of niobium, tungsten, molybdenum, aluminum, titanium and tantalum are also used. The most important properties of superalloys are

1. To maintain their strength at temperatures above 650°C,
2. Having high temperature corrosion and erosion resistance.

Superalloys; It has been classified according to its widespread use today, including iron, chromium and nickel. This classification includes complex iron-nickel-chromium cobalt compositions, cobalt-based alloys reinforced with carbides, solid

solution-strengthened nickel-based alloys, and precipitation-distribution-hardened nickel-based alloys.

It is also known that the resistances of complex alloys such as iron-nickel-chromium-cobalt alloys, iron-based alloys and nickel-based solid solution reinforced alloys are lower than their strengths at temperatures above 650°C compared to cobalt-based and nickel-based (second strength) alloys. Depending on their melting points, the strength of cobalt-based alloys at temperatures above 1100°C is higher than nickel alloys. Cobalt-based cast alloys have a face-centered cubic crystal structure and complex carbides are formed in their matrices. These materials are used for air blowers in gas turbine engines [4].

Table 1.1: Effect of elements on superalloys [5]

Elemental Effects	Fe-based	Co-based	Ni-based
Solid-melt Strengtheners	Mo, Cr	Mo, Ta, Cr, Nb, Ni, W,	Co, Cr, Mo, Fe, W, Ta
Matrix stabilizers of face-centered cubic (FCC)	Ni, C, Co	Ni	Co
Carbide types;			
MC type		Ti, Cr, Mo, W	
M <sub>7</sub> C <sub>3</sub> type		C, N	
M <sub>23</sub> C <sub>6</sub> type		W, Ta, Ti, Mo, Nb, Cr	
M <sub>6</sub> C type		Cr, Mo, W	
Carbonitrides;			
M(CN) type		Mo, W, C, N	
General precipitants of carbides	P	--	--
$\gamma'$ Ni <sub>3</sub> (Al, Ti)	Al, Ni, Ti	--	Al, Ti
Hexagonal $\eta$ (Ni <sub>3</sub> Ti) conversion retarders	Al, Zr	--	--
Increases the solvent temperature of $\gamma'$	--	--	Co
Lowers the solvent temperature of $\gamma'$	--	--	Cr
Hardening precipitants and/or intermetallics	Al, Ti, Nb	W, Al, Mo, Ta	Al, Ti, Nb
Oxidation resistance	Cr	Al, Cr, Ta	Al, Cr, Ta
Hot corrosion resistance enhancers	La, Y	La, Y, Th	La, Th
Sulfidation resistance	Cr	Cr	Cr
Enhancers of creep-rupture properties by grain boundary morphology variables	B	B, Zr	B, Zr
Intermediate-temperature ductility enhancers	--	--	Hf
Causes of grain boundary segregation	--	--	B, C, Zr

## 1.2.3 Classification of Superalloys

### 1.2.3.1 Iron-based Superalloys

The main element of iron-based alloys is iron. It contains high proportions of chromium, nickel and very low proportions of molybdenum and tungsten. This group of carbide is strengthened by intermetallic precipitation and/or solid-melt. The intermetallic precipitate is generally  $\text{Ni}_3(\text{Al,Ti})$   $\gamma'$  type. Nickel-chromium ratios and strengthening mechanisms of this group are different from stainless steels. Stainless steels contain 12-25% Cr and 0-20% Ni, while iron-based superalloys contain more than 20% Ni (25-35%) [6].

Although there are many high-iron superalloys, not all alloys are categorized as iron-based superalloys. Because these superalloys are combined of elements such as iron, nickel, cobalt, high amount of chromium and smaller amounts of niobium, molybdenum, tungsten according to their role and effects in the alloy.

Modifications are made to the alloy to improve the properties of superalloys. These modifications are carried out by adding different elements in different proportions. The most effective strengthening for matrix alloys with KYM is made with nickel, aluminum, tantalum and niobium. Some elements, such as molybdenum and tungsten, are added into the solid-melt during the strengthening stages. KYM alloys are hardened by the addition of carbon. This hardening effect can be increased by adding nitrogen and phosphorus. Carbon also increases the strength by forming grain boundary carbide at the grain boundaries. For carbide precipitation, the carbide content should be about 0.5% [7].



Table 1.2: Major phase types formed in superalloys [8]

Phase	Crystal Structure	Formula	Descriptions
$\gamma'$	KYM	$\text{Ni}_3\text{Al}$ $\text{Ni}_3(\text{Al}, \text{Ti})$	A major strengthening step in many nickel and nickel-iron-based superalloys, the crystal lattices in the austenite matrix are small, ranging in shape from spherical to cubic, and change with temperature and time.
$\eta$	HSP	$\text{Ni}_3\text{Ti}$	It is found in superalloys after prolonged exposure to high titanium/aluminum ratios.
$\gamma''$	BCT	$\text{Ni}_3\text{Nb}$	It is the main strengthening phase in Inconel 718; is a stable phase.
$\text{Ni}_3\text{Nb}$ ( $\delta$ )	Orthorhombic	$\text{Ni}_3\text{Nb}$	Over-aging is observed in Inconel 718; It has a needle-like appearance when shaped between 815 and 980°C; It is formed by intragranular precipitants at high aging temperatures and by porous reactions at low aging temperatures.
MC	Cubic	TiC, NbC, HfC	Titanium carbide phase type has solubility for molybdenum, zirconium, nitrogen elements; its composition is different; seen spherically, the "M" elements can be Ti, Ta, Hf, Nb, Th and Zr.
$\text{M}_{23}\text{C}_6$	KYM	$(\text{Cr}, \text{Fe}, \text{W}, \text{Mo})_{23}\text{C}_6$	The way of precipitation is important; the film can be deposited as spherical, plate, lamella and cellular; it is usually formed at grain boundaries; The element "M" is usually Cr, but Ni-Co, Fe, Mo and Tu can also be substituted.
$\text{M}_6\text{C}$	KYM	$\text{Fe}_3\text{Mo}_3\text{C}$ , $\text{Fe}_3\text{W}_3\text{C}$ , $\text{Fe}_3\text{Nb}_3$ $\text{Ta}_3\text{Co}_3\text{C}$	They are randomly dispersed carbides; may appear pinkish; The "M" element is usually Mo, Tu.
$\text{M}_7\text{C}_3$	Hexagonal	$\text{Cr}_7\text{C}_3$	It usually appears as an intergranular block; It occurs in some cobalt-based alloys after exposure to temperatures above 1000°C.
$\text{M}_3\text{M}_2$	Tetragonal	$\text{Nb}_3\text{B}_2$ , $(\text{Mo}, \text{Ti}, \text{Cr}, \text{Ni}, \text{Fe})_3\text{B}_2$ , $\text{Ta}_3\text{B}_2$ , $\text{V}_3\text{B}_2$ ,	About 0.03% or more is observed in B, Fe-Ni, and nickel-based alloys; borides are similar to carbides; The "M" elements can be Mo, Ta, Nb, Ni, Fe and V.
MN	Cubic	$(\text{Ti}, \text{Nb}, \text{Zr})\text{N}$ , $(\text{Ti}, \text{Nb}, \text{Zr})\text{CN}$	Nitride occurs in alloys containing Ti, Nb and Zr; they do not melt at temperatures below their melting point; They have a rectangular shaped area and available in a variety of colors from yellow to orange.
$\mu$	Rhombohedral	$(\text{Fe}, \text{Co})_7(\text{MoW})_6$	It usually occurs in alloys with a high Mo den and Tungsten content; They are in the form of rough, irregular Widmanstent plates and are formed at high temperatures.
Laves	Hexagonal	$\text{Fe}_2\text{Nb}$ , $\text{Fe}_2\text{Ti}$ , $\text{Fe}_2\text{Mo}$ , $\text{Co}_2\text{Ta}$ , $\text{Co}_2\text{Ti}$	It is very common in Fe and Co based superalloys; It is usually seen as irregular spheres forming and in the form of plates at high temperatures.
$\sigma$	Tetragonal	$\text{FeCr}$ , $\text{FeCrMo}$ , $\text{CrFeMoNi}$ , $\text{CrCo}$ , $\text{CrNiMo}$	It is mostly seen in Fe and Co-based superalloys and to a lesser extent in Ni-based superalloys. Their shapes are irregular spheres; They take shape after being kept for a long time at temperatures between 540-980°C.

Oxidation resistance is generally provided by the chromium element. However, nickel and manganese also increase oxidation resistance. With the attendance of a low ratio amount of boron element, the resistance against high temperature is increased. The most important feature of ferrous alloys for temperature applications above 504°C is that they are KYM. Because a closed-pack cage is more resistant. The first uses of iron-based superalloys strengthened by intermetallic compound precipitate are blades, discs and binders in gas turbine engines [9].

### 1.2.3.2 Cobalt-based Superalloys

The base element of cobalt-based superalloys is cobalt. It also contains a large amount of nickel, chromium, tungsten and relatively small amounts of molybdenum, niobium, tantalum, titanium and iron, depending on ambient conditions and usage areas. Cobalt-based superalloys are strengthened with the aid of solid melt and carbide phases.

Cobalt-based superalloys are classified into three groups:

- a) Alloy used at temperatures from 650°C to 1150°C
- b) Fastener alloys used at approximately 650°C
- c) Wear resistant alloys.

Because all cobalt-based superalloys contain secondary carbide phases or intermetallic compounds, none are completely solid melt alloys. This causes aging and also loss of ductility at room temperature. Generally, all cobalt-based superalloys have KYM crystal structure during heat treatment and softening [10].

### 1.2.3.3 Nickel-based Superalloys

Nickel-based superalloys contain 30 to 70% Ni as the main alloying element and a significant amount of Cr above 30% [11]. Some nickel-based superalloys also include low rate of niobium, molybdenum, aluminum, titanium, and tungsten for strength resistance and corrosion resistance.



Figure 1.1: Gas turbine engine using nickel-based superalloys effectively [12]

Nickel-based superalloys are strengthened by the secondary phase intermetallic precipitate and solid melt by the action of the elements aluminum, titanium and niobium.

The presence and interaction of nickel and chromium elements increase the oxidation resistance of nickel-based superalloys. Nickel-based superalloys are superior to stainless steels in terms of mechanical strength, especially at temperatures above 650°C [13].

Another application area of nickel-based superalloys is known as energy generators. In nuclear power plants; It is widely used for structural components of steam generating tubes and reactor cores, as well as for heater tubes in fossil fuel plants, ash removal systems and parts that need high temperature corrosion resistance.

Solid-melt nickel alloys are used at annealing temperature and annealing tempering. The low annealing temperature of 870-980°C provides the highest ductility and fatigue strength. A high temperature annealing of 1120-1200°C provides optimum fatigue resistance and creep-rupture properties at operating temperatures greater than 600°C [14].

Deposition-resistant nickel alloys are obtained by precipitation of a second phase. The most important factor in increasing the hardness and strength of the alloy is the precipitated phases (usually  $\gamma'$  or  $\gamma''$ ). In most of these alloys, aluminum and titanium are used for precipitation-hardening by shaping the  $\gamma'$  intermetallic  $\text{Ni}_3(\text{Al,Ti})$  phase. Some alloys use niobium alongside aluminum and titanium. As a result,  $\gamma''$   $\text{Ni}_3\text{Nb}$  is

formed. The presence of the niobium element delays reaching the precipitation hardening temperature. The weldability of these alloys is high because pre-weld cracking is not observed, as the weld temperature does not harden.

The most critical application of slump-resistant superalloys is in the aerospace industry. In addition, these superalloys are used in rocket engines, discs, shafts, rings, propeller blades among aircraft turbine parts, bolts and springs used in various compressors and nuclear reactors [15]

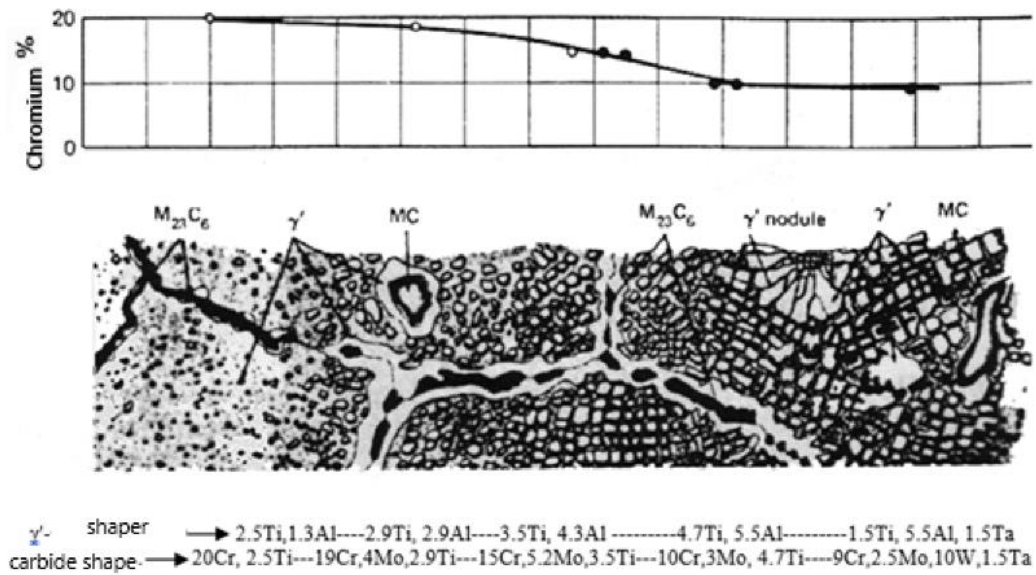


Figure 1.2: Chromium containing nickel-based superalloys and microstructural evaluation [16]

### 1.2.4 Inconel 738 and Inconel 738LC Alloys

Inconel 738 nickel-based superalloy is one of the alloys with a high usage rate, developed and patented by Inconel Corporation in 1969, produced using the traditional casting method [17]. The design of the Inconel 738 alloy was made with the aim of being used in aircraft gas turbines to resist oxidation, corrosion and stress in high temperature environmental conditions.

When the production stages of Inconel 738 are examined, it is a nickel-based alloy that can be precipitation hardened by precision casting methods under vacuum after melting under vacuum. This alloy has significant high-temperature creep-rupture resistance in addition to oxidation resistance in a high-temperature environment, which is superior to many high-strength superalloys with a low chromium content. Inconel 738 alloy has been designed for the gas turbine industry to provide an alloy that will resist the high temperature used in engine components, not immediately depleting its service life in corrosive environments, and have good creep resistance up to 982°C [18]. Inconel 738 alloy is divided into two classes as high carbon and low carbon.

Table 1.3: Chemical compositions of alloy Inconel 738 [19]

Element	Inconel 738C		Inconel 738LC	
	Range	Nominal	Range	Nominal
Carbon	0.15-0.20	0.17	0.09-0.13	0.11
Cobalt	8.00-9.00	8.50	3.00-9.00	8.50
Chromium	15.70-16.30	16.00	15.70-16.30	16.00
Molybdenum	1.50-2.00	1.75	1.50-2.00	1.75
Tungsten	2.40-2.80	2.60	2.40-2.80	2.60
Tantalum	1.50-2.00	1.75	1.50-2.00	1.75
Columbium (Niobium)	0.60-1.10	0.90	0.60-1.10	0.90
Aluminum	3.20-3.70	3.40	3.20-3.70	3.40
Titanium	3.20-3.70	3.40	3.20-3.70	3.40
Aluminum + Titanium	6.50-7.20	6.80	6.50-7.20	6.80
Boron	0.005-0.015	0.010	0.007-0.012	0.010
Zirconium	0.05-0.15	0.10	0.03-0.08	0.05
Iron	0.05 max	-	0.05 max	-
Manganese	0.02 max	-	0.02 max	-
Silicon	0.30 max	-	0.30 max	-
Sulfur	0.015 max	-	0.015 max	-
Nickel	Bal.	Bal. (61)	Bal.	Bal. (61)

Inconel 738LC is a nickel-based superalloy commonly used in turbine nozzles and turbine blades in aircraft gas turbines. Inconel 738LC, which is frequently used in gas turbine engine components, is exposed to high temperatures and high corrosion. Therefore, high temperature oxidation resistance, high temperature tensile strength, yield strength, creep resistance data and corrosion resistance of this material are of great importance.

Inconel 738LC has an extraordinary design with a combination of phase stability, corrosion resistance and high temperature resistance, which corresponds to the optimum adjustment of the elemental ratios (Cr. Mo. Co. Al. W. and Ta) in it.

The high temperature resistance of Inconel 738LC is related to the asset of the L12 type sequential  $\text{Ni}_3(\text{Al,Ti})\text{C}$  intermetallic FCC phase in the solid solution matrix of the element carbon. However, in Inconel 738LC, the high volume fraction of the element carbon increases some mechanical properties of this superalloy, but the element carbon significantly affects and reduces the weldability of Inconel 738LC. In relation to the weldability ability, it has been found that the soldered joints are affected by the presence of eutectic microstructures that are hard and brittle during the assembly operation.

As a result of the combination of liquid phase bonding and diffusion bonding techniques, the Temporary Liquid Phase (TLP) bonding method has been developed as a different another technique for joining and repairing superalloys with low weldability. In the temporary liquid phase bonding method, a filler metal consisting of elements that play an active role in melting point lowering (MPD) leaks between the substrate layers. The entire alloy is then heated to a temperature in the range of filler metal fluid and base alloy fluid.

There are generally four different steps during the TLP binding process; dissolution of the base alloy, expansion of the interlayer, isothermal solidification of the liquid, and homogenization of the bond zone. If the time to bonding is not sufficient to complete isothermal solidification, construction of eutectic structures occurs along the boundary. These components cause the mechanical values to decrease in the

border regions. Therefore, in order to obtain reliable TLP bonded connections on the Inconel 738LC, various process parameters must be properly selected.

Low carbon ratio should be preferred in Inconel 738 for better castability in large scale productions. Mechanical properties such as tensile and stress-fracture are not significantly affected by the low carbon content. Zirconium levels are kept low for better castability in Inconel 738LC. The microstructure contains the  $\gamma'(\text{Ni}_3(\text{Ti}, \text{Al}))$  intermetallic phase, which contributes to the material's defining properties. Solid solution elements available are chromium, cobalt, tungsten and tantalum; They contribute equally to the structural stability of Inconel 738LC. In addition to the decrease in porosity with increasing sintering temperature; density, hardness and predicted yield strength increase. Thermal conductivity, an important thermophysical property of Inconel 738LC, allows this alloy to increase its useful life and is preferred in high temperature applications [20].

### 1.2.5 Manufacturing Methods of Superalloy Parts

Over the years, developments in superalloy production methods and chemical compositions have led to significant increases in superalloy service temperatures. Superalloys were first produced on an iron-only basis and by cold forging prior to the 1940s. Investment casting of cobalt-based alloys in the 1940s notably increased service temperatures. With the development of vacuum induction melting in the 1950s, the chemical composition and trace elements of superalloys could be controlled. Thus began a new era in manufacturing techniques such as the directional solidification of alloys and single-crystal superalloys.

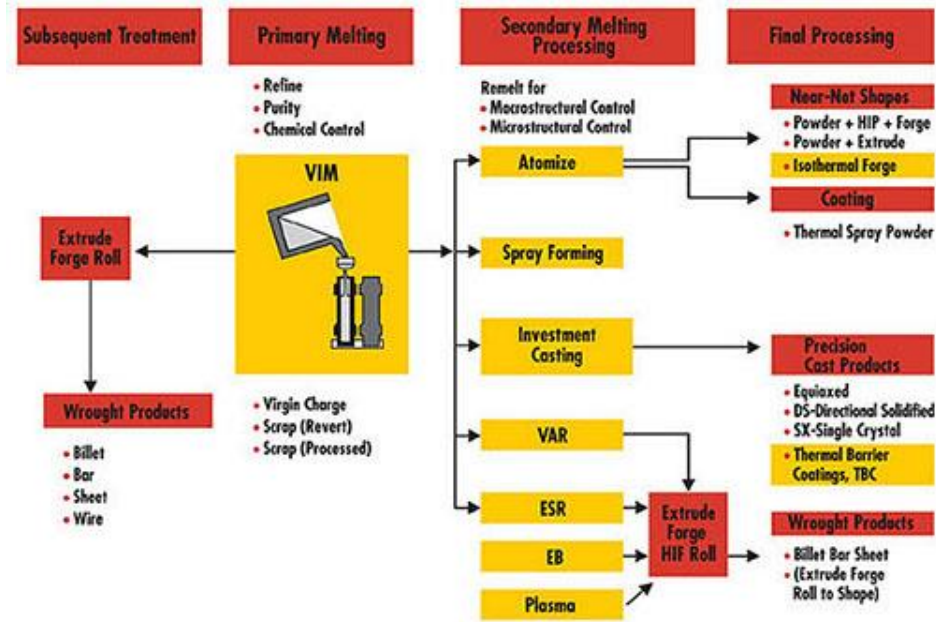


Figure 1.3: Processing routes for superalloys [21]

A variety of many types of superalloys used in a gas turbine engine, and machining methods vary depending on the key properties of each part [22].

### 1.2.5.1 Vacuum Induction Melting (VIM)

Vacuum melting is a studied and approved process for melting liquid metal in an induction-heated crucible. The first use of the production method dates back to the middle of the 19th century, but the development of the technique took place in the second half of the 20th century. Commercial vacuum induction melting (VIM) took the lead in the early 1950s with the requisition produce superalloys containing reactive elements under vacuum to prevent reactive element loss [23]. While the process is considered relatively flexible, it allows induction mixing of the melt with pressure and mass control, depending on time, temperature. Therefore, VIM offers more control options than other vacuum melting processes in terms of chemical composition requirements and homogeneous distribution of the elements in the alloy.

The vacuum induction melting process is the first preferred process in the production methods of superalloys. Compared to open atmosphere melting processes such as



argon oxygen decarburization (AOD), converter electric arc furnaces (EAF), VIM of superalloys provides a significant advantage in removing unwanted elements such as oxygen, nitrogen and hydrogen. Accordingly, with less oxide and nitride formation, the microstructure cleanliness and mechanical properties of vacuum melted superalloys are greatly improved compared to superalloys melted in open atmosphere.

#### 1.2.5.2 Investment Casting

Investment casting consists of a series of processes using liquid refractory slurry. In this casting method, a disposable (reusable) model is used, which is surrounded by liquid refractory material at room temperature. For this model, wax or plastic is usually used. If we examine the general lines of the process: Wax or plastic, including shrinkage tolerances, a mold is pressed to give the desired shape. Models prepared in this way are arranged in clusters around the runner. This inflorescence is covered with a thin refractory. The wax is taken out by melting and this fine refractory is sintered at around 1000°C. This formed shell is cast while it is hot. Then the ceramic shell is broken and cast in the form of a cluster is taken, the remaining ceramics are cleaned, the runner and nozzles are cleaned. The surface of the piece obtained is very clean compared to other casting methods and does not need to be processed [24].

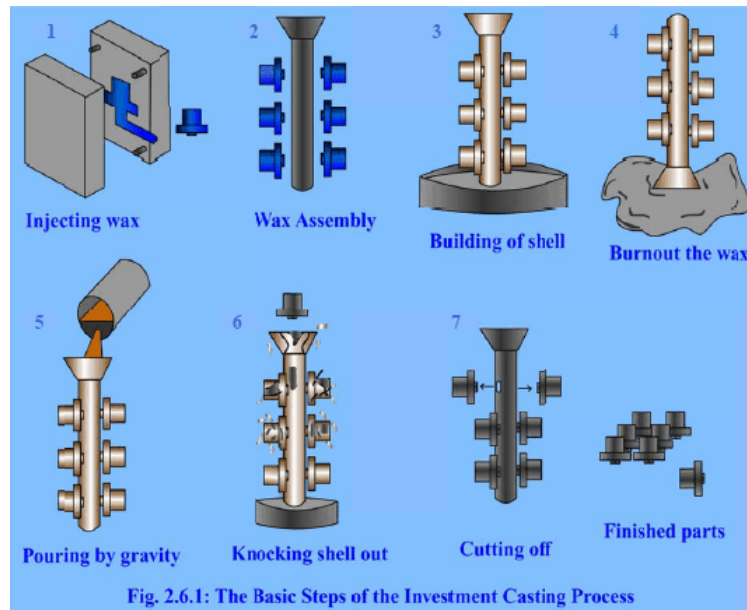


Figure 1.4: Steps in investment casting process [25]

### 1.2.5.3 Heat Treatment

Heat treatment processes applied to superalloys include precipitation hardening, stress relieving, intermediate or full annealing, solution treatment, or diffusion of coatings. The full annealing process is used to obtain a completely recrystallized, soft and ductile structure. Inter-process annealing can be used to reduce residual stress in the material after welding or between different forming operations. The solution process is done to dissolve the second phases. Additional solute may be used for precipitation hardening in this process. Precipitation hardening (the common name in the industry is age hardening) is used to expose reinforcing mechanisms, including carbides and topologically closely packed structures [26].

### 1.2.6 Coatings for Superalloys

Most of the coatings applied to superalloy components are applied to protect the base material from adverse environmental conditions and the negative effects of these conditions. Coating is also applied to extend the life of materials operating at 1010 °C and higher temperatures for a longer period of time. The protective coating is a layer of material that prevents direct interaction between the base material and harmful environmental conditions. The adverse effects of environmental conditions

can be in the form of deformation of the metal from oxidation and corrosion, or in the form of a decrease in mechanical properties due to high temperature diffusion of deformed surface impurities into the substrate. Most protective coatings are designed to protect the substrate, the superalloy base material, from these effects and extend its life.

Among the high temperature coatings for superalloys, the two most commonly used methods are as follows; diffusion and overlay coatings. These methods are used to protect the base material from oxidation and corrosion. The thermal barrier coating method, which is one of the other methods, is applied to protect the substrate from thermal deformation. All coating types are designed to prevent exposure to hot gas or direct interaction between harmful environmental components and the base metal alloy. This design aims to extend the life of high temperature applications that are often subject to corrosion or thermal deformation [27].

Table 1.4: Relationship between coating functions and coating material characteristics

Coating function	Coating material characteristics
Lowering the surface temperature	Low thermal conductivity coefficient, Low radiant heat transfer, High diffusion coefficient,
Reducing the oxidation rate	Thermodynamically stable oxide formation with a low growth rate,
Increasing hot corrosion resistance	Chemically stable, impermeable oxide layer,
Resistance to particle erosion	Hard, dense coating material
High wearability	Friction-tolerant material with plastic deformation (condensation), Energy conversion capability with fracture (material loss),
High abrasiveness	Presence of hard particles to increase cutting ability,

Most coatings applied to superalloys are not designed to be compatible with the base material; This expression means that they are not inert coatings. These coatings have different chemical and physical properties than the material they protect. By reacting

with environmental oxygen between aluminum and chromium elements, superalloy coatings form a dense and very tight oxide layer that prevents the diffusion of trace elements such as nitrogen or sulfur into the base material. The coatings must contain enough reactive elements such as aluminum, chromium and silicon to maintain the protective layer continuously. At the same time, the coating should be moderately compatible with the base material.

For the compatibility of the coating and the base material, it is important to use the appropriate application technique and the coating materials that reduce the unwanted reactions between the coating material and the base material and the diffusion of the coating elements to the base surface. These problems can cause material defects, such as cracking or void formation, which reduce the mechanical values of the superalloy. Differences in thermal expansion rates can also create incompatibility, so coatings with a certain degree of ductility are generally more effective.

Several types of coating processes are applied for superalloy products exposed to high temperature working environments and corrosive environments. These transactions are; The package cementation process is gas-phase deposition (the two methods are known as chemical vapor deposition (CVD), thermal sputtering, and physical vapor deposition.

High spray particle velocities are used in the HVOF coating process. Due to the very high particle velocities, the coating has a high density. In addition, the coating applied to the material surface has very little porosity. Additionally, it is a highly variable system, as spray parameters can be altered depending on the material used and the desired coating quality. The coatings obtained offer limitless possibilities for industrial use.

The HVOF system is an application of the flame spray method and is suitable for using materials that can only be accumulated in powder form. In the HVOF thermal spray method, the material in powder form is melted with the heat generated by the combustion of a gas acting as fuel with oxygen and is sprayed onto the surface to be coated at very high speeds with the help of compressed air. The powders are exposed to flames in the combustion chamber and become molten or semi-molten depending on their melting points and the rate of powder feeding.

Scope of application:

- In Aircraft Industry: Turbine Blades
- In Paper Industry: Drying Rollers, Scraper Blades.
- In the Textile Industry: Polymer Blades
- In Wire Drawing Industry: Wire Drawing Reels, Heads, Stepped Pulleys.
- In the Petrochemical Industry: Packing Bushes, Piston Rods, Gate Valves.
- In the Tire Industry: Banburi Mixers.

A gas or liquid fuel mixture is fed with oxygen to the combustion chamber and combustion is achieved by ignition. Fuels can be gas (hydrogen, methane, propane, propylene, acetylene, natural gas, etc.) or liquid (kerosene, etc.). The hot gas, which has a pressure close to 1 MPa, is ejected from the combustion chamber through a smaller diameter nozzle at high pressure and velocity due to combustion. The velocity at the nozzle exit is approximately 1000 m/s higher than the speed of sound. The powder injected into the gas stream is sprayed out of the nozzle, accelerating up to 800 m/s. It is ensured that the hot gas and powder flow is directed towards the surface to be coated. The powder partially melts during flow and settles on the substrate. At the end of the coating, it has low porosity and high bond strength.

HVOF coatings can be applied up to 12 mm thickness. Metallic and carbide coatings are typically applied to obtain surfaces with wear and corrosion resistance. Commonly used powders are WC-Co, chromium carbide, MCrAlY and alumina. The most successful coating applications of this method are known as carbide applications (WC-Co etc.) and other corrosion resistant alloys. (stainless steels, nickel-based alloys, aluminum) [28].

HVOF spraying system has superior features, including;

- high adhesion strength,
- high density,
- low porosity,
- high hardness (Tungsten Carbide 1300 HV),
- ideal corrosion resistance,
- unique wear resistance (abrasion, adhesion),
- homogeneous structure, smooth surface,
- good machinability (turning, grinding, lapping, honing, superfinish polishing),
- low oxidation, and minimum foreign material.

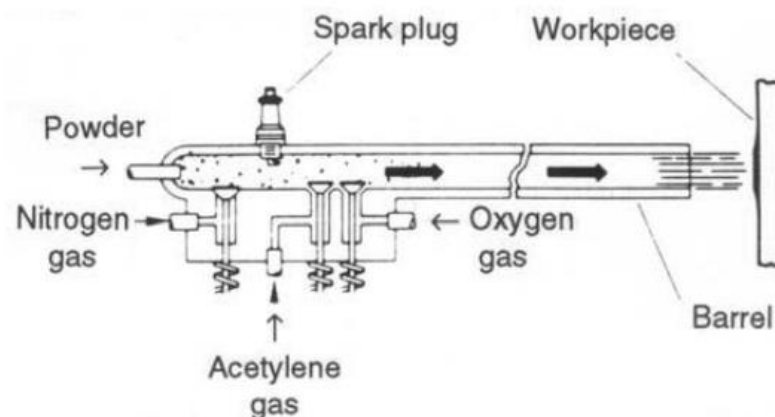


Figure 1.5: HVOF process [29]

### 1.2.7 High Temperature Oxidation (Hot Corrosion)

High temperature oxidation (also known as hot corrosion) is one of prevalent time-lapse oxidation processes. The biggest reason is due to environmental pollutants such as salt or sulfur in the fuel. The chromium content in most cobalt, nickel, and iron-based superalloys is usually sufficient to prevent hot corrosion. However, for some types of nickel-based superalloys, especially those with higher fracture strength at higher temperatures, this has a negative effect. Protective coatings, particularly

plating coatings and sometimes environmental inhibitors are required to protect high-strength nickel-based superalloys [31].

Hot corrosion is a highly deforming type of damage in high temperature applications. In hot corrosion, molten salts react very easily with reactive components and cause premature damage to workpieces. Hot corrosion is usually caused by the presence of trace elements such as Na, S, V and Cl in a gas turbine due to gases formed in hot ambient conditions. Hot corrosion; It occurs in two different forms, Type I, which is High Temperature Hot Corrosion (HTHC), and Type II, which is Low temperature Hot Corrosion (LTHC). High Temperature Hot Corrosion is normally observed in the temperature range of 825–950°C when the condensed phase is clearly liquid [32].

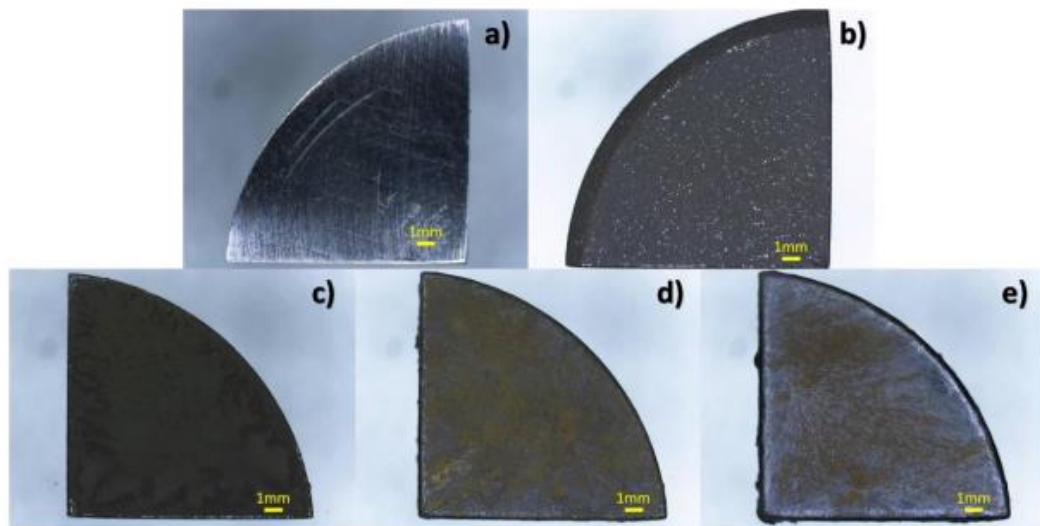


Figure 1.6: For Inconel 718 material a) before high temperature oxidation test, b) isothermal after 18 hours, c) after 6 hours (1st cycle), d) after 12 hours (2nd cycle) and e) after 18 hours (3rd cycle) macro images[33]

One of the elements in the alloy of the coating material may diffuse into the base metal, which may have an effect on the initial melting temperature of the metal. When a superalloy is heated beyond its initial melting point, it causes a decrease in grain boundary strength and ductility. After this heat treatment, it is not possible to recover the material properties in terms of mechanical and microstructural properties. While the high temperature oxidation and hot corrosion limit is usually determined

by considering the upper temperature limit for a superalloy, it can often be preferred to use forged materials used without protective coating in applications at lower temperatures than this limit, such as rotary seals or turbine discs, while preserving their mechanical properties [34].

## 1.2.8 Literature Overview

Al-Jarba et al. (2004) showed the effect of carbon was added to nickel-based superalloys to reduce grain defects. It has been observed that the tendency of the alloy to form all kinds of solidification defects decreases with the increase of carbon content. Also, as the carbon ratio increased, there was a decrease in the ratio of  $\gamma$ - $\gamma'$  eutectic structure in the final casting microstructure and an increase in the volume fraction and porosity of the carbides. The carbides formed in these alloys are mostly MC type carbides that form dendritic networks in interdendritic regions. With the increase of the carbon content, the initial melting point drops significantly and the carbide morphology has changed from blocky to letter-like. The dissociation behavior of Tungsten and Tantalum is also affected by the small addition of carbon. Low carbon addition also affects casting shrinkage and eutectic structure formation [35].

LIU. studied that (2004), the carbon level also changes the behavior of the other elements in the alloy and their effect on the alloy. In the elemental ratios in the investigated chemical composition, the addition of carbon results in the formation of two types of tantalum-rich carbide morphology: blocky and writing-like. The addition of carbon to this single-crystal superalloy is effective in causing shrinkage and reduction of the eutectic content. Due to the addition of carbon, the decomposition of element Ta and W is markedly reduced. At the same time, the addition of carbon is detrimental to the alloy by lowering its incipient melting point and preventing complete dissolution of the  $\gamma'$  phase. Intentional carbon additions lead to the formation of Tantalum-rich MC carbides during solidification and change the decomposition behavior of the constituent elements [36].

F. S. Pettit and G. H. Meier studied in their work (1984), when discussing the effects of alloying elements on hot corrosion of superalloys, it is necessary to relate the comments to an appropriate mode of propagation. Because some elements can



produce harmful effects for one mode of propagation and beneficial for another. Carbide phases are the first regions to initiate deformation in hot corrosion attack and thus represent an undesirable situation in terms of hot corrosion resistance [37].

Subhash Kamal and coworkers found that (2010), oxidation and hot corrosion create problems in terms of service life in gas turbines with aircraft, marine, industrial and land-based use. This is due to the use of a wide variety of fuels, with increased operating temperatures leading to deterioration of turbine engines. Alloys produced to eliminate these problems; Superalloys (Midhani grade) such as Superni 75, Superni 718 and Superfer 800H are prominent materials for high temperature applications. It is critical to investigate the degradation mechanism of superalloys due to oxidation and hot corrosion and to prove the effect of alloying elements in the formation of protective oxide films on their surfaces for these superalloys. Therefore, it is the subject of this study to investigate the oxidation and hot corrosion resistance of superalloys exposed to air and molten salt ( $\text{Na}_2\text{SO}_4$ -60%  $\text{V}_2\text{O}_5$ ), respectively, at  $900^\circ\text{C}$  under cyclic conditions. Parabolic rate constants calculated for superalloys show that the corrosion rate in air is minimal compared to a molten salt environment [38].

K. V Sharma and coworkers found that (2017), hot corrosion occurs by excitation of metals in the temperature range of  $700$ – $900^\circ\text{C}$  in the presence of sulfate deposits formed as a result of the reaction of gaseous sodium chloride and sulfur mixtures in the working environment of metals. While there are some alloys that resist the steps of hot corrosion from the initial stage to the diffusion stage, no alloy can resist hot corrosion formation indefinitely. Superalloys are produced to work in high temperature ambient conditions. However, these alloys should not be exposed to hot corrosion because they cannot maintain both high temperature resistance and high temperature corrosion resistance simultaneously. In order for the material to be protected against high temperature, many conditions must be met. These are; It should be resistant to high environmental conditions, the base material and the coating should be chemically and mechanically compatible, practically applicable, reliable and economically preferable [39].

# Chapter 2

## Materials and Methods

### 2.1 Material and Production Process

Castings in the composition of Inconel 738 (0.15-0.20% C) and Inconel 738LC (0.09-0.13%) were produced using the VARZENE METAL vacuum induction furnace. According to the carbon values in the ranges determined according to the suitability of the post-cast chemical analysis results, four ingots as seen in Table 2.1 and 2.2 were determined from both high carbon Inconel 738 ingots and low carbon Inconel 738LC ingots.

Table 2.1: Chemical composition of the produced Inconel 738 ingot (0.19% C)

Element	Composition % weight	Element	Composition % weight
C	0.19	Ti	3.20-3.70
Mn	max 0.20	Ta	1.50-2.00
Si	max 0.30	Al	3.20-3.70
P	max 0.015	B	0.005-0.015
S	max 0.015	Zr	0.025-0.08
Cr	15.70-16.30	Fe	max 0.50
Co	8.00-9.00	Cu	max 0.10
Mo	1.50-2.00	Ni	remainder
W	2.40-2.80	Nb	0.60-1.10

Table 2.2: Chemical composition of the produced Inconel 738LC ingot (0.13% C)

Element	Composition % weight	Element	Composition % weight
C	0.13	Ti	3.49
Mn	0.0072	Ta	1.81
Si	0.0432	Al	3.39
P	0.0045	B	0.012
S	<0.00070	Zr	0.0460
Cr	15.79	Fe	0.301
Co	8.51	Cu	0.0132
Mo	1.83	Ni	61,4
W	2.75	Nb	0.760



Figure 2.1: Ingots for investment casting

Initially, 4 ingots of high carbon Inconel 738 alloy were sent to GÜR METAL Investment Casting company Ankara, ingot for blank production by investment casting production method. For the investment casting process, at least 20 kg of ingot should be used. The surface of 4 pieces of ingot is ground and made ready for investment casting. The ingots were cast as tensile test coupons in investment casting as indicated in Figure 2.2.



Figure 2.2: Blank sample produced by vacuum investment casting

The produced blank sample dimensions are as follows in accordance with the standards top and bottom: Ø15.6 mm, Gauge area: Ø7.7 mm, Length: 146 mm.

## 2.2 Heat Treatment Process

After the investment casting process, the blank samples are subjected to solution and aging heat treatments. In the heat treatment process, the most appropriate parameters were determined by considering the literature reviews.

The solution heat treatment was applied in vacuum, usually between 980°C and 1350°C, and is then cooled to room temperature with a fast gas fan. First of all, the alloy is brought to the convenient temperature and stayed at that temperature for a while, one or more compounds are formed and mixed into the solid solution. Finally, it is cooled at such a rate that the components remain in solution. This is the solution process. After the solution process, an artificial aging process is applied under the conditions given in Table 2.3.

Table 2.3: Solution and aging heat treatments parameters

Type of the treatment	Temperature °C	Duration (hours)	Cooling procedure
Solution heat treatment	1121°C	2	GFQ
Aging heat treatment	843°C	24	Cool at any rate to room temperature

## 2.3 HVOF Thermal Spray Coating

High speed oxy fuel injection technique (HVOF) was preferred as the coating process. Two different powder mixtures were prepared as coating material and applied on the material. In order for the coatings to spread better on the sample surface, 24 grit aluminum oxide powder was processed with the sandblasting

machine shown in Figure 2.4 with the sandblasting method. The powder mixtures that were used in the HVOF process are as follows;

- $\text{Cr}_2\text{Co}_3\text{-}20\text{NiCr}$
- $(\text{WC-}12\text{Co})\text{-}33(\text{Cr}_2\text{C}_3\text{-}20\text{NiCr})$



Figure 2.3: Sandblasting machine

The mineral aluminum oxide is formed due to the high sensitivity of aluminum metal to oxygen. They are preferred in the surface treatment sector due to their high hardness and durability. They are the most commonly used materials in paint removal or roughening processes. Aluminum oxide is widely used in roughening before coating due to its high hardness and angular structure. When they are sprayed on the surface with compressed air, they form micron-level cracks on the surface depending on the size of the abrasive material. When a coating process is applied later, the coating material that settles into these cracks adheres better to the base metal, increasing the coating life and quality.



Figure 2.4: Sample surfaces after the aluminum oxide sandblasting

The brown aluminum oxide content consists of less than 1.5% free silica and is therefore safer to use than sand. The grain size is consistent and cuts much faster than sand, leaving a smoother surface. In general, the larger the grain size, the faster the aluminum oxide blast medium will cut. Fine grained aluminum oxide powder was preferred to prepare the ground for the main coating. Due to the smoothness of the main surface, coarse-grained aluminum oxide coating was not required.



Figure 2.5: HVOF process

As with all thermal sputtering processes, the coating material is heated and directed to the surface of the part via a gas stream to continue the process. With the HVOF process, the gas stream was produced where oxygen and fuel (gas or liquid) were mixed in a combustion chamber and ignited as shown in Figure 2.5 followed by a rapid jet of high pressure gas from a nozzle. The powder was introduced into this stream where it was heated and sprayed against the surface of the part. The final coating was in the form of thin overlapping platelets.

## 2.4 Characterization Studies

### 2.4.1 Mechanical Testing

The tensile test is one of the most common tests to determine the strength properties of materials in the field of engineering. By applying tensile forces on the sample from opposite faces in the same direction, it is possible to determine the characteristic values for yield point or yield stress, tensile strength and elongation at break. Room temperature tensile test was performed according to ASTM E8 standard.

High temperature tensile testing is a method in which tensile testing is used together with the heating process to investigate the efficacy of high temperatures and stress on tensile strength and material properties. Many industries, such as the energy sector, aviation and automotive, are in search of materials suitable for ambient conditions that can withstand high temperature conditions. Components such as pistons, turbine blades, and valves operate in high-temperature environments in the course of use and require the materials that make up the components to be tough enough to withstand these extreme use and environmental conditions without deforming. High temperature tensile tests were carried out according to ASTM E21.





Figure 2.6: Tensile test samples

The purpose of the tensile test applied at high temperatures is to investigate the behavior of the material in the environment where it is planned to work, to examine the mechanical and thermal properties of the material and to observe the change in the microstructure of the material. This test is also seen as a comparative evaluation method for strength and ductility [41].

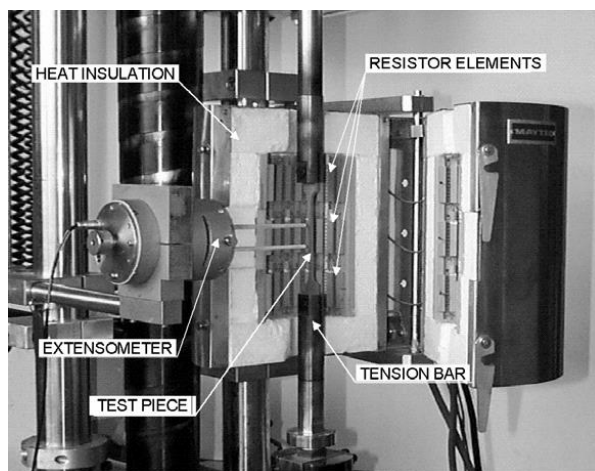


Figure 2.7: High-temperature tensile testing device [42]

The tensile rupture test is applied to determine the time it takes for the material to deform by subjecting it to a constant load at a constant temperature. The test measures the breaking time and the effect of temperature on long-term load-bearing properties. The results are of enormous importance in the selection of materials where dimensional tolerances are not critical, but rupture is not allowed. The tensile rupture test is almost identical to the creep test except that the stress ratios are higher [43]. Stress rupture tests were performed according to ASTM E139 standard.

### 2.4.2 Microstructural Study

The samples were cut in appropriate sizes and mounted. After sanding and polishing, it was examined under an optical microscope. Photographs were taken under an optical microscope using different magnifications.

### 2.4.3 High Temperature Oxidation Tests

High temperature oxidation tests were carried out at 850 °C and 1000 °C in the electric resistant heat treatment furnace within the Varzene Metal Superalloy Test Laboratory.



Figure 2.8: Electric resistance heat treatment furnace

Initially, the samples were kept in the oven for 16 hours for both temperatures. At the end of 16. hours, the samples were taken out of the oven and allowed to cool in air. A precision balance with 0.01-gram sensitivity was used to look at the weight gains of the samples falling to room temperature.



Figure 2.9: Placement of samples in the furnace

Again, isothermal heat treatment periods were completed as 24 hours, 32 hours and 40 hours, respectively, with 8 hour cycles for both temperatures. After each 8-hour cycle, the cooling and subsequent weight gains were checked. In addition to the furnace thermocouple, temperature controls were made during the process by using external K-type calibrated thermocouples for each heat treatment.

#### 2.4.4 Scanning Electron Microscopy (SEM) Analysis

SEM is a kind of electron microscope that can take view from the sample surface by scanning a focused electron beam. Electrons interact with sample atoms to generate signals to differ from each other.

These signals are detected by the detectors and give information about the sample surface map and the chemical composition content of the alloy.

Secondary electrons (SE; secondary electron) emitted by the sample atoms by being excited by the electron beam are generally used to obtain images in SEM. The difference in the number of secondary electrons emitted from different parts of the

sample initially depends on the angle of contact of the beam with the surface, i.e. the state of the surface. Unlike secondary electrons, backscattered electrons (BSE), characteristic X-rays, light (electron beam) (CL), sample current and transferred electrons and various signals are taken from the sample, and appropriate surface map and chemical composition analyzes are performed [45].



Figure 2.10: Scanning electron microscopy (SEM)

For oxidation resistance,  $\text{Ø}16*15$  mm samples were cut using a hand saw from the parts whose heat treatment was completed. The samples were taken sequentially at the Sample Preparation and Metallography Laboratory of Katip Çelebi University. The surfaces of the samples were smoothed by using 80, 320, 1200 and 2000 grit sandpapers, respectively. After the sanding process, the sample surfaces were polished with polishing paper using detergent water.

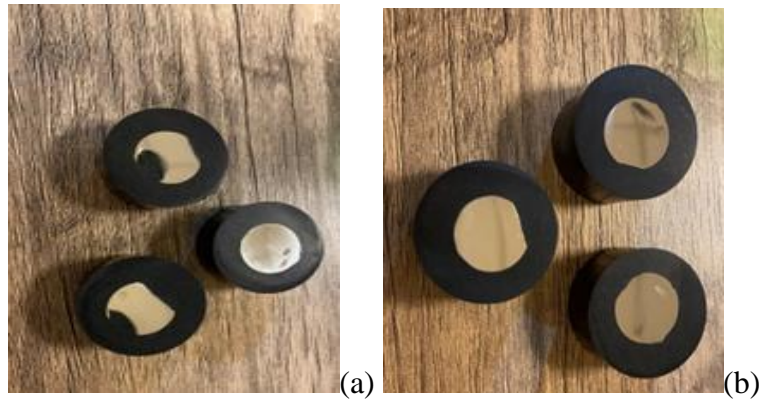


Figure 2.11: SEM samples undergone to oxidation tests (a) at 850 °C, (b) at 1000°C

# Chapter 3

## Results and Discussion

### 3.1 Mechanical Test Results

#### 3.1.1 Stress Rupture Test Results

According to the results of the stress rupture tests performed at 982°C for Inconel 738 alloy samples, which are shown in Table 3.1, the rupture time was found to be approximately 37.8 hours. However, the average rupture time has found to be 42.6 hours for low-C samples (as shown in Table 3.2), which corresponds to an increase of 12.7% in the average rupture time. It shows that the increase in carbon ratio in high temperature environments yield in a lower life. However, with the decrease of carbon ratio, a decrease of 15.8% was observed in the mean elongation value (from 16.1 to 13.9%). It can be said that the increase in carbon ratio increases the yield and tensile strength of the steel and it decreases the percent elongation value. As can be seen from the results, the average percent elongation value increased with higher carbon ratio in Inconel 738 superalloy. Normally, increasing C content increases the stress rupture properties such as rupture time. This is because the higher carbon content decreases the eutectic content of the alloy and it also increases the grain size and thus decreases grain boundaries. However, in our case the higher carbon ratio yields lower life but higher elongation. As can be seen from the Tables 3.1 and 3.2 that the standart deviation of the rupture time values is higher for the lower-Carbon samples which means that the values are quite similar. For the elongation values, the higher-Carbon samples show higher elongations which is expected as the eutectic content is lower and also the grain size is smaller in our findings (Jiang).

Table 3.1: Stress rupture test results of Inconel 738 (0.19% C) samples

Sample No	Temperature (°C)	Stress (MPa)	Rupture Time (hour)	Elongation (%)	
IN738 Sample 1	982	151	33.3	13.3	
IN738 Sample 2	982	151	37.7	15	
IN738 Sample 3	982	151	42.3	20	
Average			37.8	16.1	
Test Requirements (according to the ASTM E139 standard)		982	151	Min. 30	Min. 5

Table 3.2: Stress rupture test results of Inconel 738 (0.13% C) samples

Sample No	Temperature (°C)	Stress (MPa)	Rupture Time (hour)	Elongation (%)	
IN738LC Sample 1	982	151	36.9	12.5	
IN738LC Sample 2	982	151	52.5	14.2	
IN738LC Sample 3	982	151	38.3	15	
Average			42.6	13.9	
Test Requirements (according to the ASTM E139 standard)		982	151	Min. 30	Min. 5

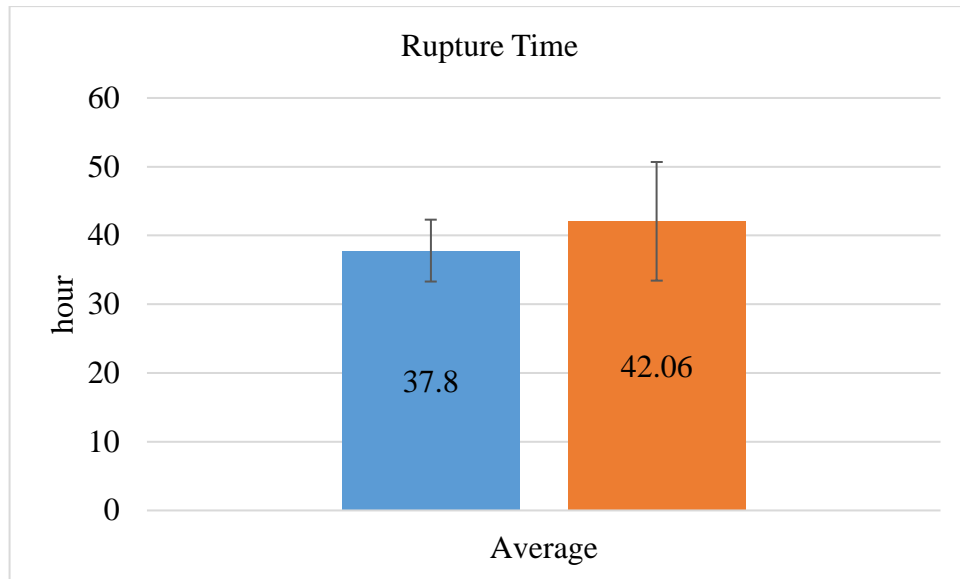


Figure 3.1: Comparative chart for stress rupture time results

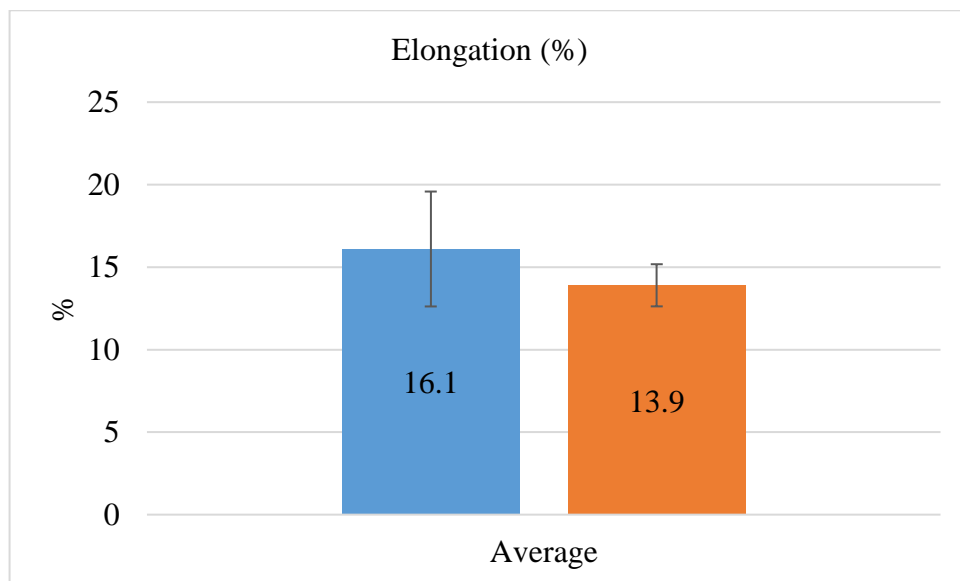


Figure 3.2: Comparative chart for stress rupture test elongation results

### 3.1.2 High Temperature Tensile Test Results

The results of the high temperature tensile tests applied to Inconel 738 high carbon samples at two different temperatures are given in Table 3.3. Bettge, D. et al. obtained 12% elongation at 750°C tensile tests in their work for the Inconel 738LC



alloy. According to the elongation values in the table, it has been interpreted that the carbon element has a negative effect on the elongation value at high temperatures, while the elongation values of low-C samples are higher than high-C samples for both temperatures. Based on the high temperature tensile test results at two different temperatures, the decrease in carbon ratio has a positive effect on the increase in strength. Considering the ultimate tensile strength and yield strength values, the strength values of IN738LC samples were higher at both temperatures. As can be seen in the graphs in Figure 3.3 and Figure 3.7 prepared for both temperatures, an increase of 3.88% was observed in the strength values. Again, in the comparative graphs of % elongation and reduction area values in Figure 3.5, Figure 3.6, Figure 3.8 and Figure 3.9, it is seen that the percentage elongation and percentage reduction in area of the low-carbon samples are higher than the high-carbon samples. Compared with the tensile rupture test results, it was observed that the decrease in carbon ratio in the high temperature tensile test results was effective in increasing the percent elongation value.

As a result, for both mechanical properties at 760 and 982°C, lower-carbon samples yield higher yield strength, tensile strength as well as elongation values. The possible reasons of this advantageous behavior could be firstly the decrease of  $\gamma$  and  $\gamma^3$  phases thus increase of MC and M<sub>6</sub>C carbides but also the decrease of grain size with the lower carbon content (0.13%). These findings are parallel with the findings of Jiang et al. as they showed that the tensile properties of the alloy decrease significantly when the carbon content is increased from 0.10 to 0.27 wt.% (Jiang).

Table 3.3: High temperature tensile test results of Inconel 738 (0.19% C) samples

Sample Number	Test Temperature	U.T.S.	0.2% Y.S.	Elong.4D	RA
IN738 Sample 1		915	749	5	10
IN738 Sample 2	760°C	946	751	10	10
IN738 Sample 3		911	720	5	10
Average		924	740	6.7	10
IN738 Sample 1		367	286	26	36
IN738 Sample 2	982°C	364	268	16	29
IN738 Sample 3		360	284	11	29
Average		364	279	17.7	31.3

Table 3.4: High temperature tensile test results of Inconel 738LC (0.13% C) samples

Sample Number	Test Temperature	U.T.S.	0.2% Y.S.	Elong.4D	RA
IN738LC Sample 1		966	776	8.75	10.94
IN738LC Sample 2	760°C	981	787	13.75	10.94
IN738LC Sample 3		964	781	10	11.53
Average		970.3	781.3	10.8	11.1
IN738LC Sample 1		378	285	35	36.84
IN738LC Sample 2	982°C	376	291	31	36.84
IN738LC Sample 3		376	284	30	36.84
Average		376.6	286.6	32	36.84

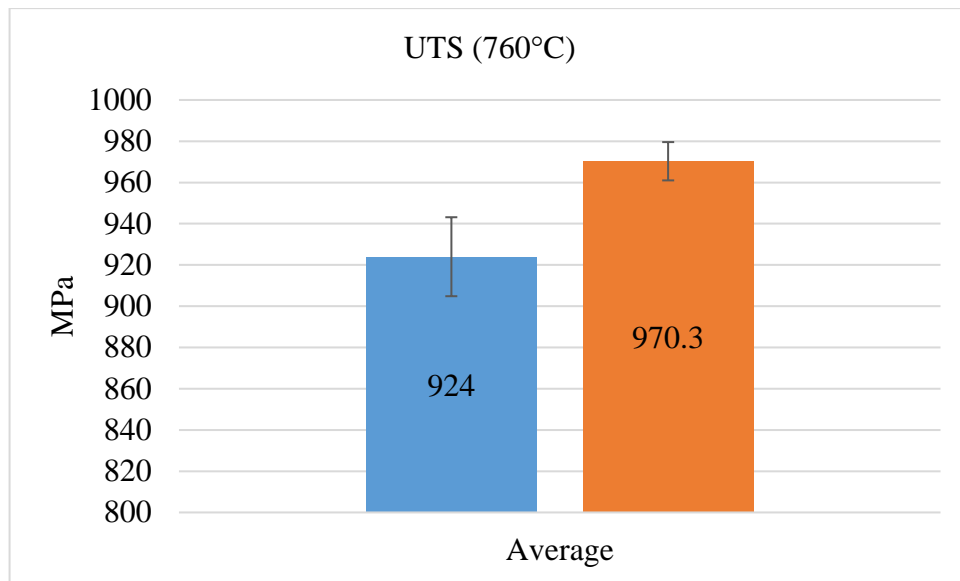


Figure 3.3: Comparison chart for 760°C high temperature ultimate tensile strength results

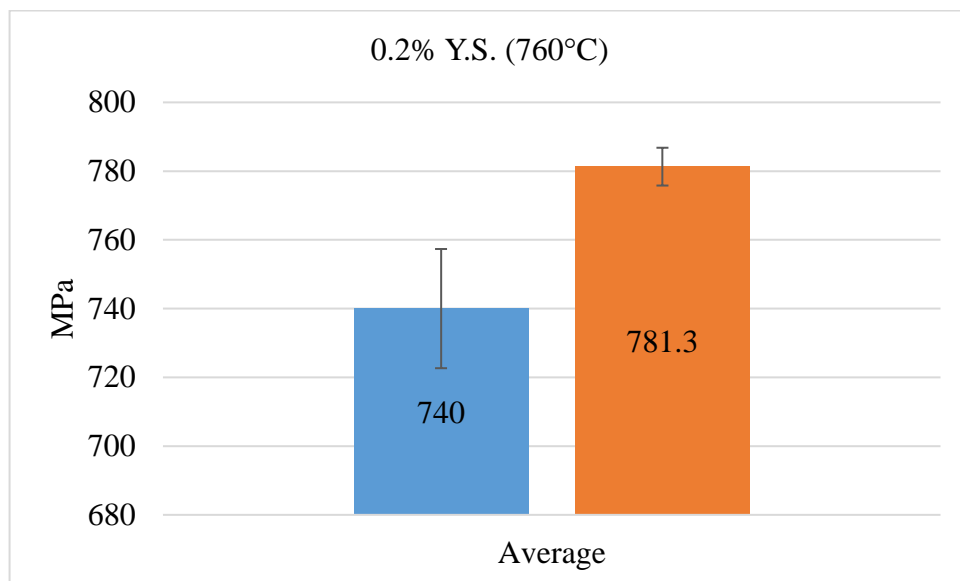


Figure 3.4: Comparison chart for 760°C high temperature yield strength results

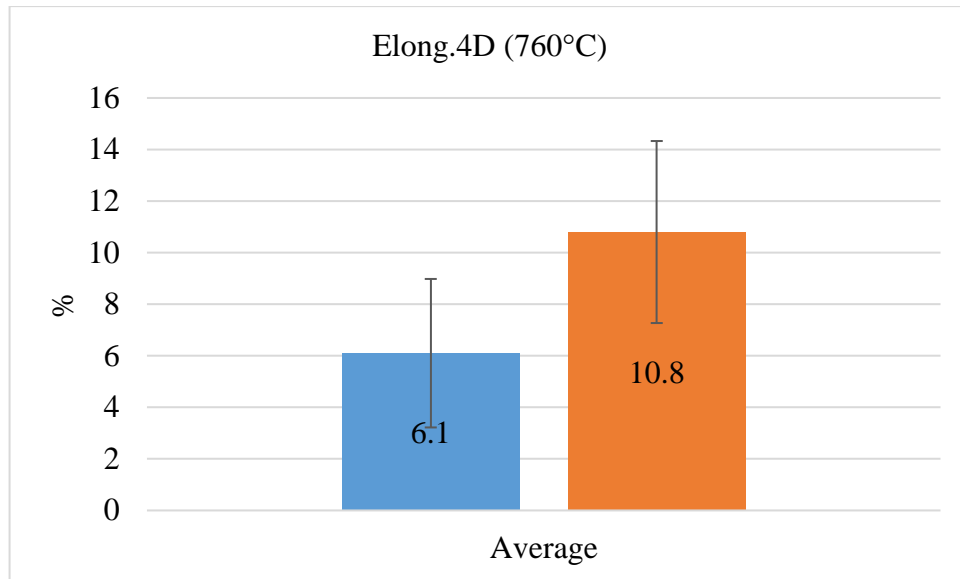


Figure 3.5: Comparison chart for 760°C high temperature elongation results

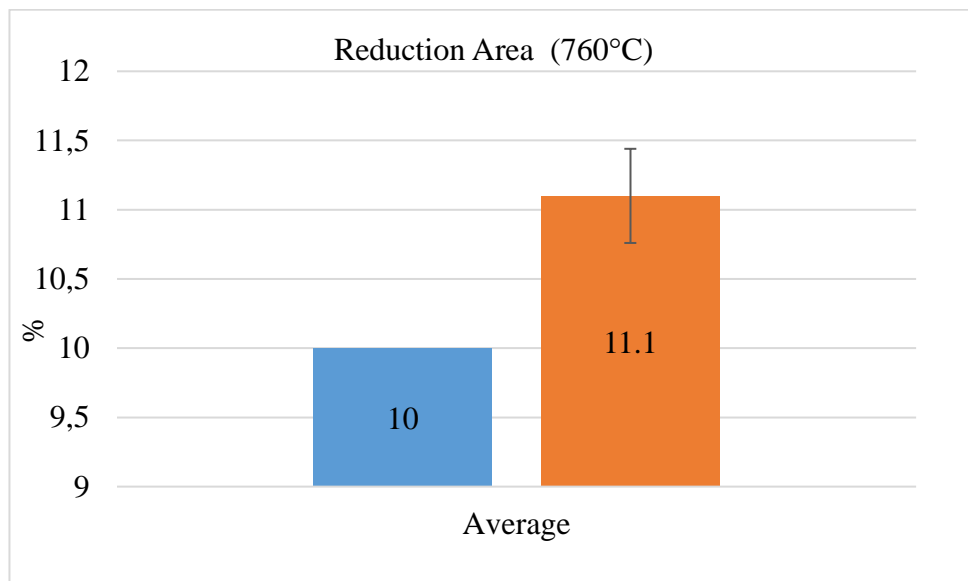


Figure 3.6: Comparison chart for 760°C high temperature reduction area results

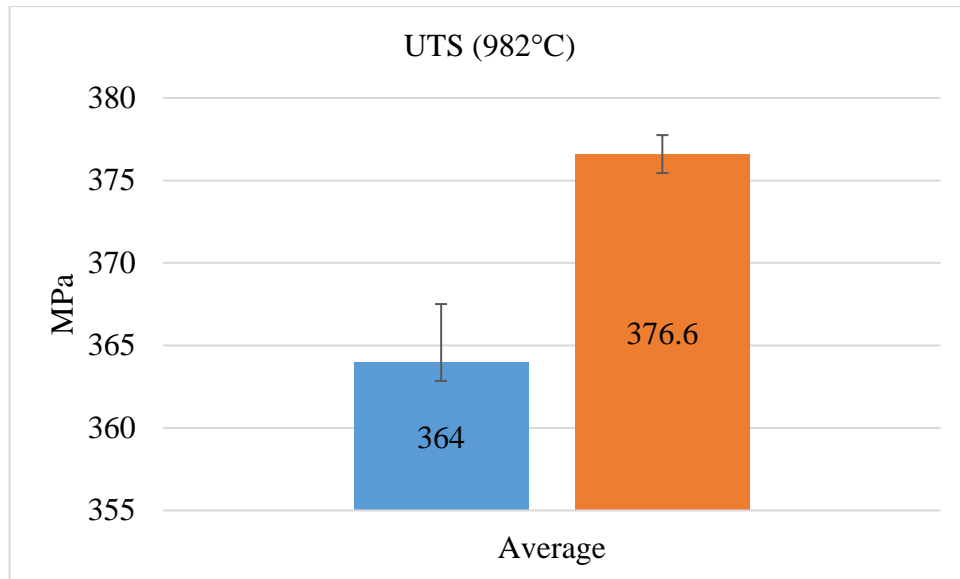


Figure 3.7: Comparison chart for 982°C high temperature ultimate tensile strength results

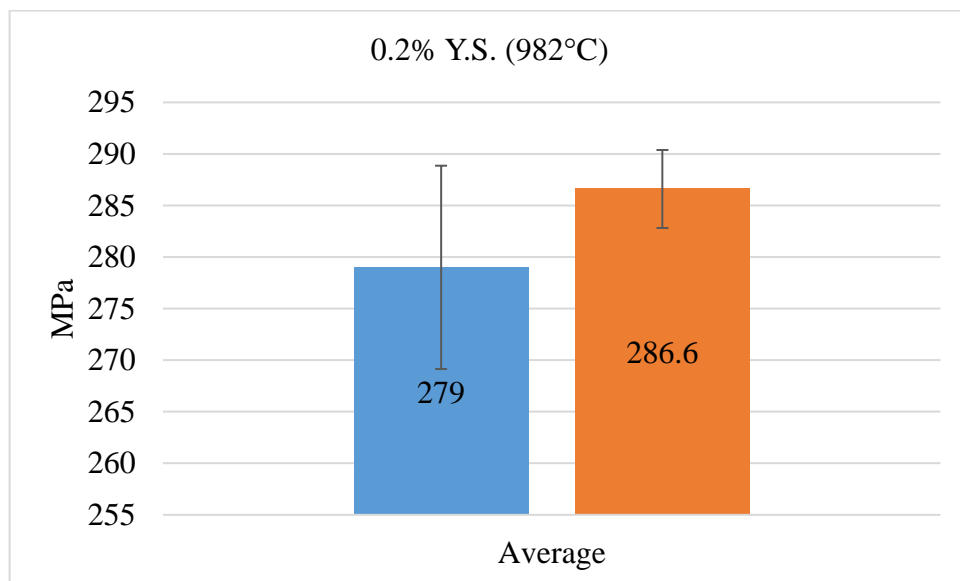


Figure 3.8: Comparison chart for 982°C high temperature yield strength results

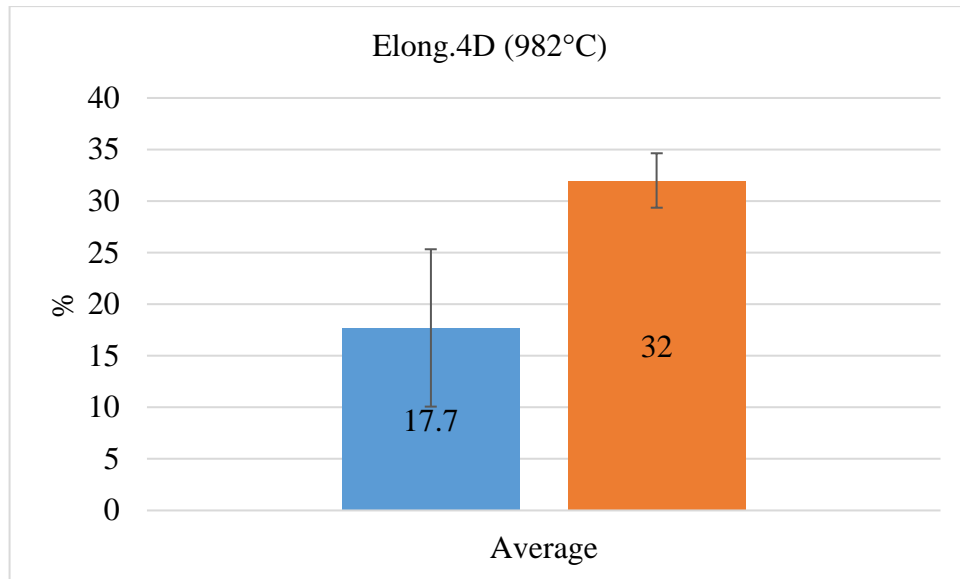


Figure 3.9: Comparison chart for 982°C high temperature elongation results

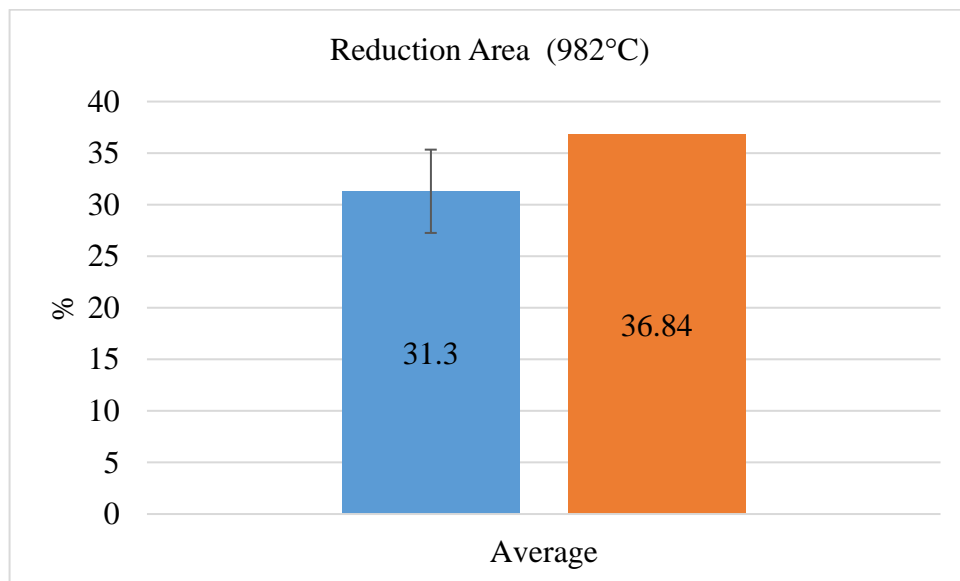


Figure 3.10: Comparison chart for 982°C high temperature reduction area results

### 3.1.3 Room Temperature Tensile Test Results

The test results applied to Inconel 738 high carbon specimens are given in Table 3.5. In the literature, the % elongation obtained in tensile tests at room temperature for Inconel 738LC alloy is 2%. As a result of the comparison of the values in the

literature and the table, the high carbon content negatively affected the elongation value in the mechanical properties. The average values of the tensile test results at room temperature and 760°C were exactly the same. The change in carbon content affects the strength values. As can be seen in the average tensile test results shown in Figure 3.11, an increase of 3.88% in the strength value was observed. As indicated in the average yield strength results in Figure 3.12, an increase of 1.33% in the strength value was observed. Again, as can be seen in the comparative graphs of % elongation and reduction area values in Figure 3.13 and Figure 3.14, it is seen that the percent elongation values of the low carbon samples are 17% higher and the cross-sectional reduction area is 12% higher than the high carbon samples. The most common carbide structures are types MC, M<sub>23</sub>C<sub>6</sub> and M<sub>6</sub>C. These carbides may precipitate during manufacture, during operation, or during heat treatment. According to the researchers, the dominant grain boundary precipitation is provided by the niobium-rich MC carbides. Although their composition is interchangeable, niobium carbides are stable. In some cases, titanium can replace niobium and form (Ti,Nb)C. In Sudararaman studies, it was found that the precipitation of carbides at the grain boundary showed that it was dependent on the aging temperature. In addition, grain boundary fracture including carbide precipitation increased with increasing aging temperature in these studies. Another point mentioned in Sudararaman's studies is that carbides at grain boundaries directly affect the crack formation type of alloys and cause intergranular defects.

In the study of Jiang et al., it is stated that C addition (as a grain boundary strengthening element), decreases the melting temperature point which results in coarser grains and it also inhibits the complete solution of  $\gamma'$  phase. Thus, the amounts of gamma and gamma prime phases decrease. Besides, with the increase in C content, the volume fraction and size of MC carbides increased, and an interdendritic network of carbides evolved more prominently. Here in our study, the lower carbon content (0.13%) not only increases eutectic phase and carbides, but also decreases grain size because of the change in solidification. Therefore, the smaller grain size yields better mechanical properties (both yield strength, tensile strength and elongation) as grain boundaries hinder dislocation motion (Jiang, Bettge).

Table 3.5: Room temperature tensile test results of Inconel 738 (0.19% C) samples

Sample Number	U.T.S. (Mpa)	0.2% Y.S. (Mpa)	Elong.4D (%)	RA (%)
IN738 Sample 1	936	803	6	7
IN738 Sample 2	915	808	5	5
IN738 Sample 3	926	802	5	5
Average	925.6	804.3	5.3	5.6

Table 3.6: Room temperature tensile test results of Inconel 738 (0.13% C) samples

Sample Number	U.T.S. (Mpa)	0.2% Y.S. (Mpa)	Elong.4D (%)	RA (%)
IN738LC Sample 1	960	815	6	5
IN738LC Sample 2	970	810	7	7
IN738LC Sample 3	955	820	5	3
Average	961.6	815	6	5

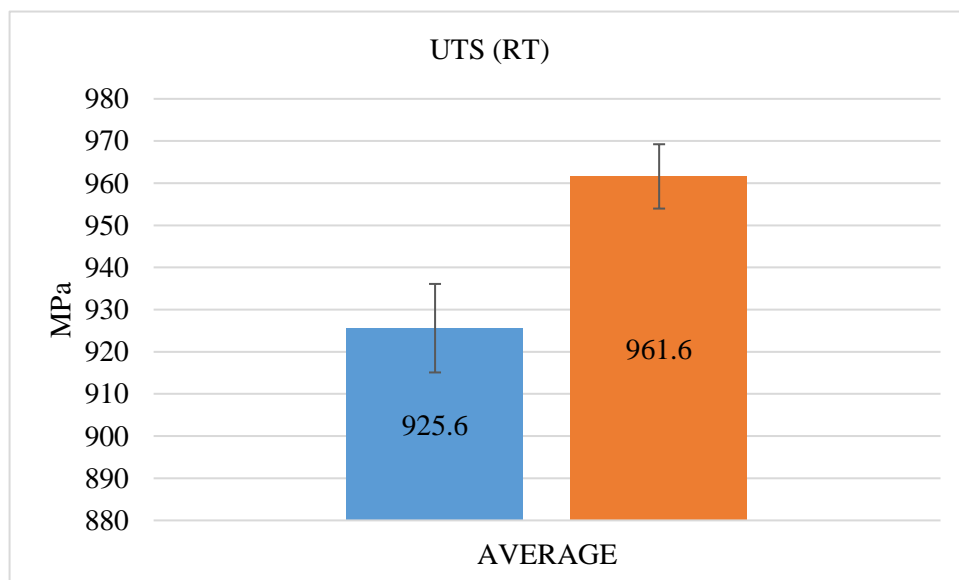


Figure 3.11: Comparison chart for room temperature ultimate tensile strength results



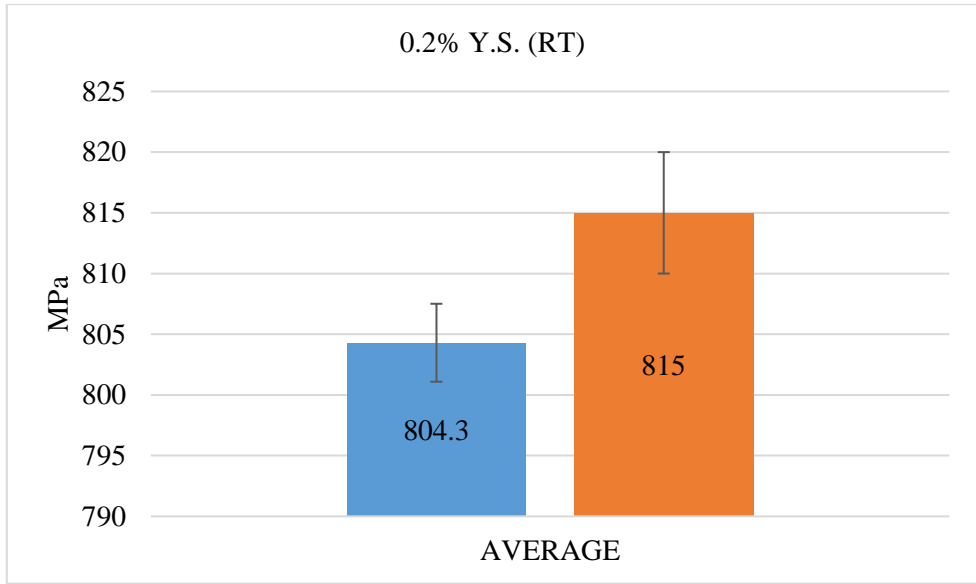


Figure 3.12: Comparison chart for room temperature yield strength results

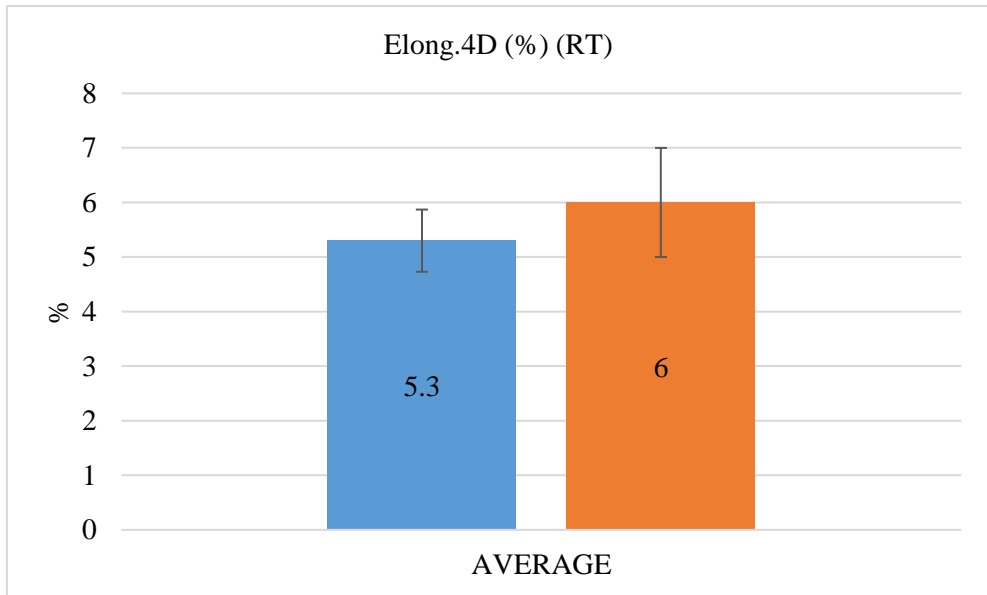


Figure 3.13: Comparison chart for room temperature elongation results

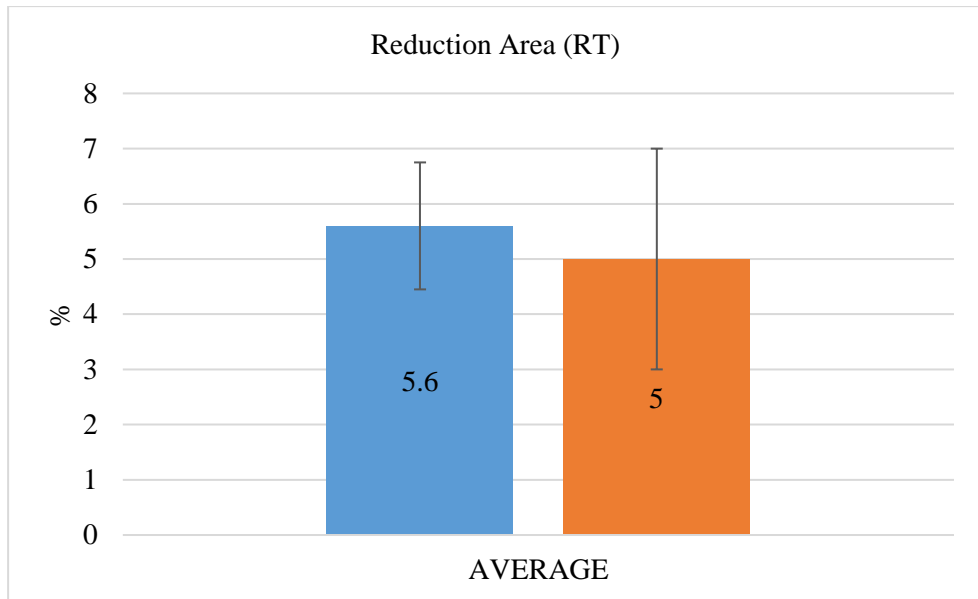


Figure 3.14: Comparison chart for room temperature reduction area results

### 3.2 Microstructural Study Results

Austenitic dendritic microstructure was observed in the microstructure examinations of the sections of Inconel 738 and Inconel 738 LC samples, as seen in Figure 3.15 and Figure 3.16. N. El-Bagoury et al. stated that they observed the same microstructure in heat treatment optimization studies. Small secondary dendritic arm spacing provides high strength and improved ductility. As a result, rapid cooling after heat treatment has a positive effect on the mechanical properties of the material.

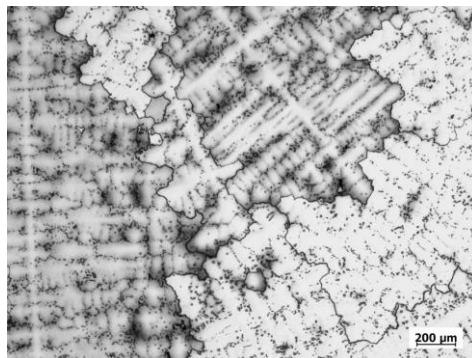


Figure 3.15: Microstructure images of IN738 sample

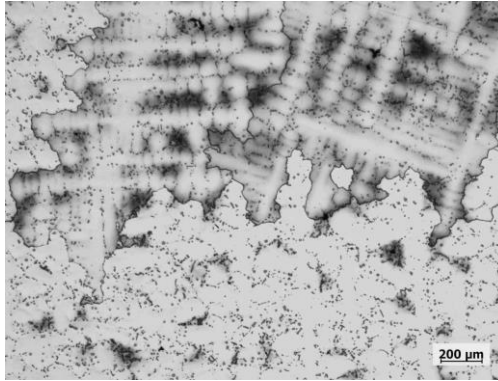


Figure 3.16: Microstructure images of IN738LC sample

In the literature, the average grain size of Inconel 738 alloys is stated as 6.5 mm as coarse grain. However, in aviation applications, fine grains and grain sizes in the 2-3 mm range are generally desired. The grain sizes in different sections of the IN738 and IN738LC samples are shown in Table 3.7. The macro grain sizes of the low carbon sample are finer than the macro grain sizes of the high carbon sample. This grain size situation is one of the reasons why it is more preferred in aviation applications.

Table 3.7: Macro grain sizes observed on sample surfaces

Sample Code	Macro Grain Size (mm)
IN738	7.75
IN738	8.58
IN738	7.14
Average	7.82
S.D.	0.72
IN738LC	5.63
IN738LC	3.42
IN738LC	6.28
Average	5.11
S.D.	1.49

### 3.3 Oxidation Test Results

#### 3.3.1 Weight Changes

The weight measurement results made between the steps of the oxidation resistance test heat treatment processes are given in the Table 3.8.

Table 3.8: Oxidation resistance test at 850°C and 1000°C temperatures weight changes due to heat treatment steps

850°C / 16 h (after step 1)	% Weight Gain	1000°C / 16 h (after step 1)	% Weight Gain
Uncoated	0	Uncoated	1.06
Cr <sub>2</sub> C <sub>3</sub> -20NiCr	0	Cr <sub>2</sub> C <sub>3</sub> -20NiCr	1.17
(WC-12Co)- 33(Cr <sub>2</sub> C <sub>3</sub> -20NiCr)	0	(WC-12Co)- 33(Cr <sub>2</sub> C <sub>3</sub> -20NiCr)	1.27
850°C / 24 h (after step 2)		1000°C / 24 h (after step 2)	
Uncoated	0	Uncoated	2.10
Cr <sub>2</sub> C <sub>3</sub> -20NiCr	0.02	Cr <sub>2</sub> C <sub>3</sub> -20NiCr	2.65
(WC-12Co)- 33(Cr <sub>2</sub> C <sub>3</sub> -20NiCr)	0.36	(WC-12Co)- 33(Cr <sub>2</sub> C <sub>3</sub> -20NiCr)	1.57
850°C / 32 h (after step 3)		1000°C / 32 h (after step 3)	
Uncoated	-0.01	Uncoated	2.15
Cr <sub>2</sub> C <sub>3</sub> -20NiCr	0.01	Cr <sub>2</sub> C <sub>3</sub> -20NiCr	3.55
(WC-12Co)- 33(Cr <sub>2</sub> C <sub>3</sub> -20NiCr)	0.96	(WC-12Co)- 33(Cr <sub>2</sub> C <sub>3</sub> -20NiCr)	3.97
850°C / 40 h (after step 4)		1000°C / 40 h (after step 1)	
Uncoated	0	Uncoated	2.66
Cr <sub>2</sub> C <sub>3</sub> -20NiCr	0.01	Cr <sub>2</sub> C <sub>3</sub> -20NiCr	4.68
(WC-12Co)- 33(Cr <sub>2</sub> C <sub>3</sub> -20NiCr)	1.02	(WC-12Co)- 33(Cr <sub>2</sub> C <sub>3</sub> -20NiCr)	2.26
850°C	Total % Weight Gain	1000°C	Total % Weight Gain
Uncoated	-0.01	Uncoated	8.21
Cr <sub>2</sub> C <sub>3</sub> -20NiCr	0.04	Cr <sub>2</sub> C <sub>3</sub> -20NiCr	12.58
(WC-12Co)- 33(Cr <sub>2</sub> C <sub>3</sub> -20NiCr)	1.69	(WC-12Co)- 33(Cr <sub>2</sub> C <sub>3</sub> -20NiCr)	9.96

It was observed that there was no weight gain in the first 2 steps in the uncoated sample at 850 °C. When the weight gains are examined after the process steps performed at 850°C; While the weight of the uncoated sample was 95.99 g before the process, it was observed that a weight loss of 0.01 g was experienced after 4 cycles. Looking at the Cr<sub>2</sub>C<sub>3</sub>-20NiCr coated sample, the weight, which was 97.97 g before the process, increased by 0.04 g. When the (WC-12Co)- 33(Cr<sub>2</sub>C<sub>3</sub>-20NiCr) coated

sample was examined, the weight, which was 95.43 before the process, increased by 1.69%.

When the weight gains are examined after the process steps performed at 1000°C; While the weight of the uncoated sample was 96.01 g before the process, it was observed that there was an 8,21 % weight increase after 4 cycles. Looking at the Cr<sub>2</sub>C<sub>3</sub>-20NiCr coated sample, the weight, which was 97.26 g before the process, increased by 12.58 %. When the (WC-12Co)- 33(Cr<sub>2</sub>C<sub>3</sub>-20NiCr) coated sample was examined, the weight, which was 99.79 before the process, increased by 9.96 %.

As can be understood from the weight gains, the oxygen affinity of the tungsten (W) combination coating alloy, known as a high temperature refractory material, is lower than the chromium combination coating. For this reason, tungsten combination coating showed a more effective function at 1000°C than chrome combination coating. The general oxidation kinetics in the chrome combination plating steps performed at 850°C are almost equal from the beginning of the oxidation. However, when the relationship of its kinetics at 1000°C with oxygen was examined, an increase in parabolic velocity was observed with an increase in temperature.

### 3.3.2 SEM Analyzes

After the oxidation test, changes in coated and uncoated samples exposed to high temperatures were analyzed by scanning electron microscopy (SEM). Capillary crack formations due to thermal stresses are remarkable on the surfaces of all three samples.

The aluminum element in the IN738LC uncoated sample composition is one of the most easily oxidized elements in the alloy content. As you can see in Figure 3.19, the aluminum oxide layer has settled on the material surface after the oxidation test. The presence of aluminum element increases the oxidation resistance in the composition. As Vedat Ç. et al observed, the precipitation of Ni<sub>3</sub>(Al, Ti) in the  $\gamma'$  phase is the most important mechanism used in the strengthening of superalloys. The increase in volume of the  $\gamma'$  phase also causes an increase in high temperature strength. Therefore, the higher the amount of aluminum and titanium in nickel-based

superalloys, the higher the high temperature strength [46]. As seen in Figure 3.17, the element carbon in the alloy is the element that interacts the most with oxygen at the closest point to the surface. As seen in Table 3.11, there has been an increase in the ratio of oxygen and carbon elements.

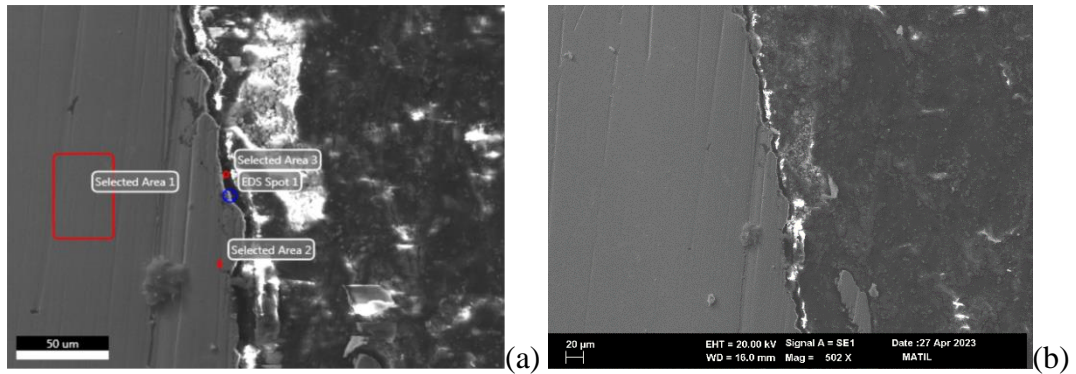


Figure 3.17: Uncoated sample images after 4 cycles of oxidation test at 850°C

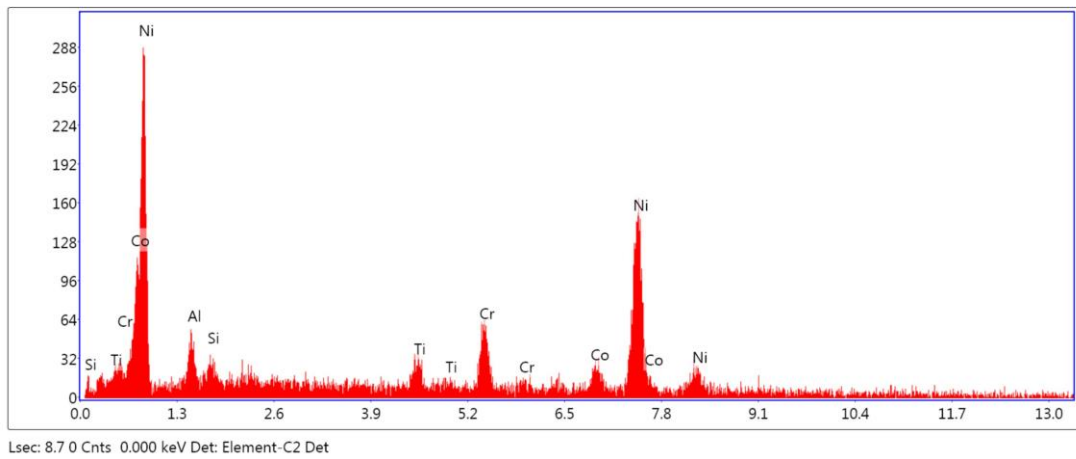


Figure 3.18: Selected area 2

Table 3.9: eZAF smart quant results of area 2

Element	Weight %	Atomic %
AlK	5.66	11.12
SiK	1.98	3.74
TiK	3.07	3.40
CrK	10.11	10.30
CoK	7.01	6.30
NiK	72.16	65.13

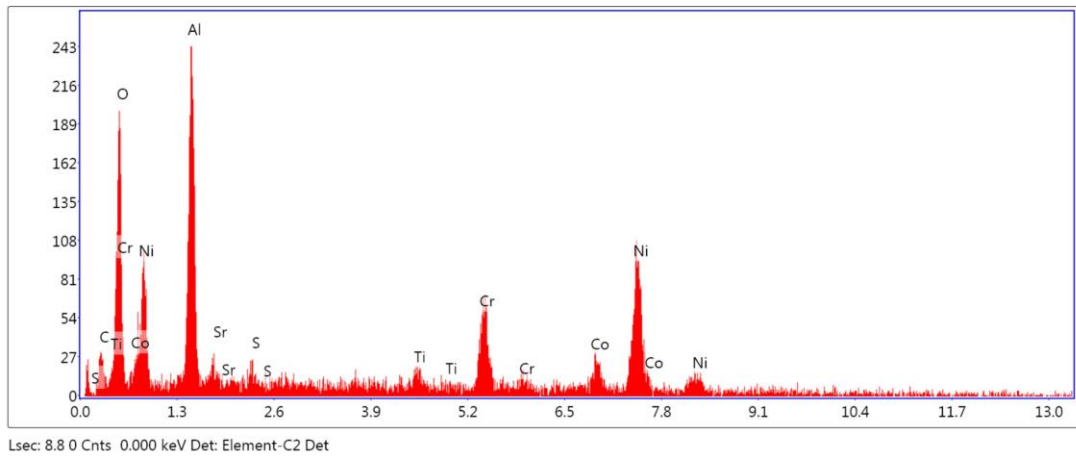


Figure 3.19: EDS spot 1





Table 3.11: eZAF smart quant results of area 3

Element	Weight %	Atomic %
C K	26.41	47.65
O K	23.26	31.51
CaK	8.75	4.73
CrK	15.97	6.65
NiK	25.62	9.46

(WC-12Co)- 33(Cr<sub>2</sub>C<sub>3</sub>-20NiCr) coating composition has been observed to interact more with oxygen due to the fact that the tungsten carbide ratio is higher than the chromium element. As seen in the elemental distribution in Figure 3.22, the oxygen element diffused into the coating interacted with the carbon. As seen in Figure 3.21, it is possible to understand the progression of carbon and oxygen interaction in the eroded coating material by oxidation test. Considering the elemental percentage in Table 3.12, it is interpreted that there is a serious wear on the tungsten carbide coating.

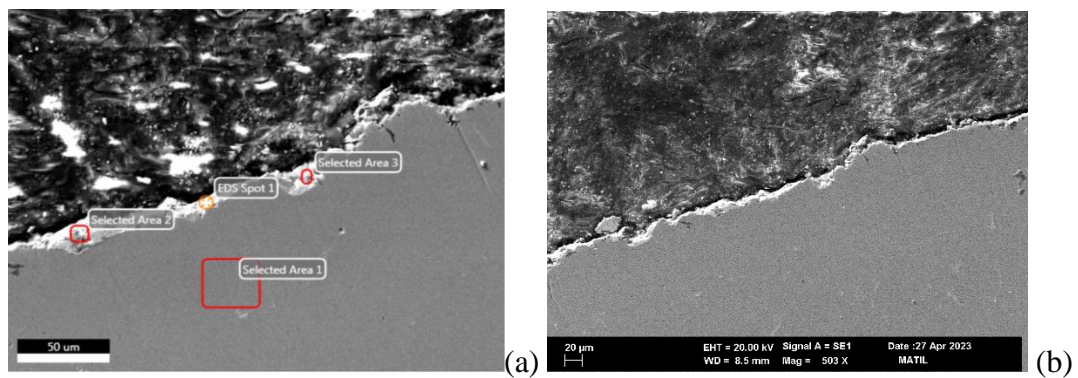


Figure 3.21: (WC-12Co)- 33(Cr<sub>2</sub>C<sub>3</sub>-20NiCr) coated sample images after 4 cycles of oxidation test at 850°C

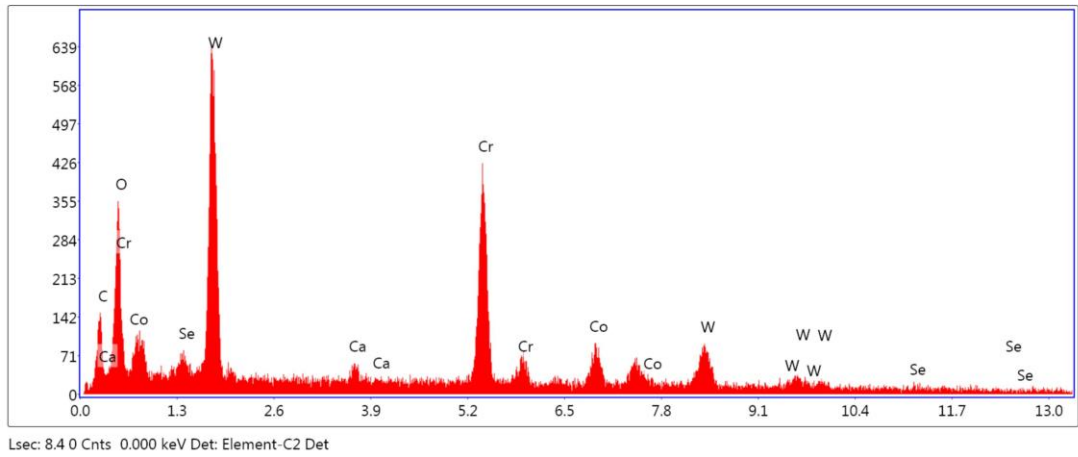


Figure 3.22: Selected area 2

Table 3.12: eZAF smart quant results of area 2

Element	Weight %	Atomic %
C K	9.02	29.97
O K	13.39	33.40
SeL	0.44	0.22
CaK	1.27	1.26
CrK	27.61	21.20
CoK	7.56	5.12
W L	40.72	8.84

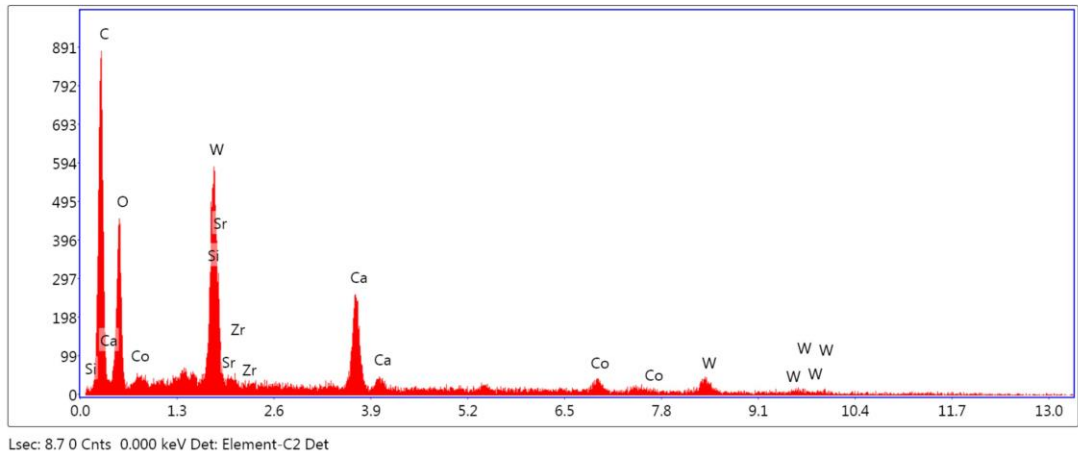


Figure 3.23: Selected area 3

Table 3.13: eZAF smart quant results of area 3

Element	Weight %	Atomic %
C K	41.03	58.80
O K	32.68	35.16
SiK	0.76	0.46
SrL	1.15	0.23
ZrL	0.01	0.00
CaK	7.65	3.28
CoK	2.49	0.73
W L	14.22	1.33

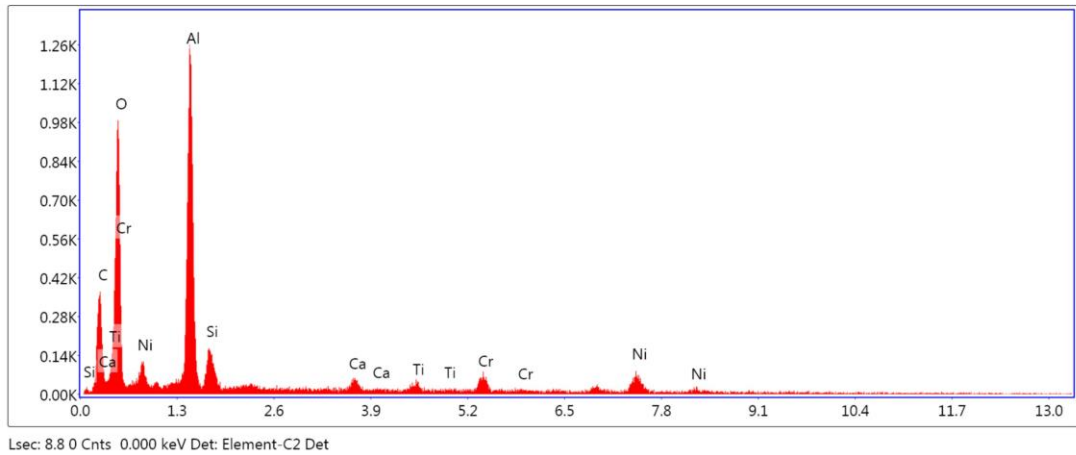


Figure 3.24: EDS spot 1

Table 3.14: eZAF smart quant results of EDS spot 1

Element	Weight %	Atomic %
C K	27.57	40.03
O K	38.54	42.02
AlK	19.19	12.40
SiK	2.65	1.65
CaK	0.98	0.43
TiK	1.05	0.38
CrK	3.01	1.01
NiK	7.01	2.08

In the  $\text{Cr}_2\text{C}_3\text{-20NiCr}$  coated sample, diffusion of chromium from the coating and carbon from the sample occurred. As a result of oxidation resistance, pits and thermal cracks were observed between the coating and the sample as seen in Figure 3.25. After the oxidation test, as a result of the corrosion of the coating material, the oxygen element moved from the coating to the sample surface. The elemental distribution in Figure 3.26 also supports this situation. As can be seen from Table 3.16, the wear rate of the  $\text{Cr}_2\text{C}_3\text{-20NiCr}$  coated sample was less than the (WC-12Co)-

33(Cr<sub>2</sub>C<sub>3</sub>-20NiCr) coated sample, due to the increased oxidation resistance of the chromium element at 850°C.

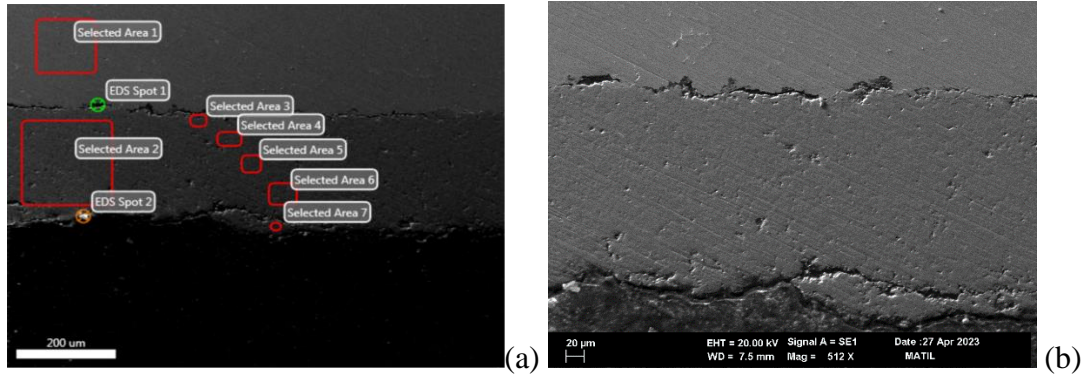


Figure 3.25: Cr<sub>2</sub>C<sub>3</sub>-20NiCr coated sample images after 4 cycles of oxidation test at 850°C

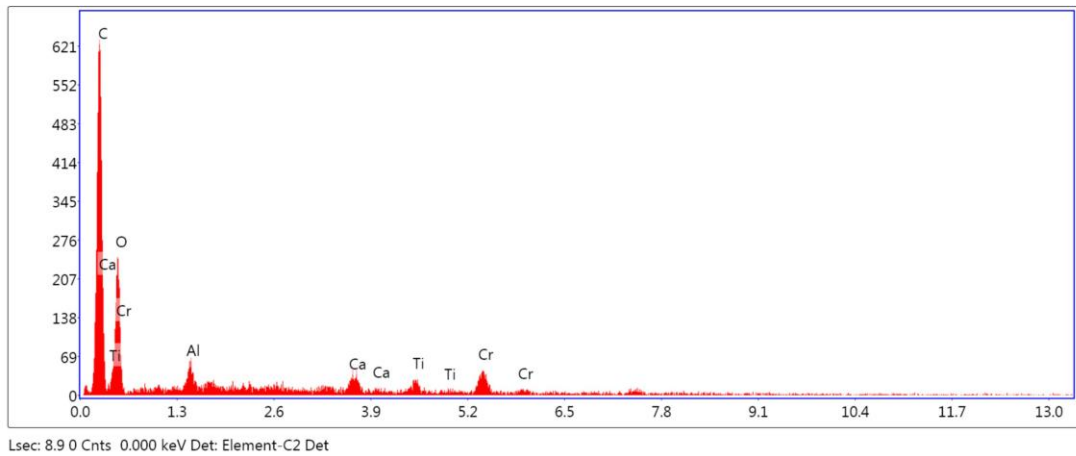


Figure 3.26: EDS spot 1

Table 3.15: eZAF smart quant results of EDS spot 1

Element	Weight %	Atomic %
C K	55.76	65.60
O K	35.99	31.78
AlK	0.85	0.44
CaK	1.74	0.61
TiK	1.27	0.37
CrK	4.40	1.19

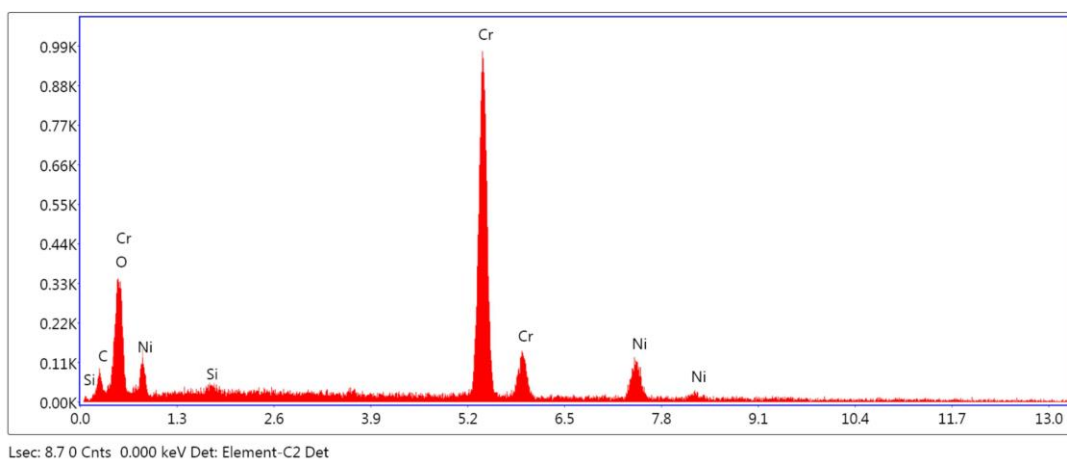


Figure 3.27: Selected area 2

Table 3.16: eZAF smart quant results of area 1

Element	Weight %	Atomic %
C K	4.45	15.83
O K	3.63	9.71
SiK	0.71	1.08
CrK	74.11	60.93
NiK	17.10	12.45

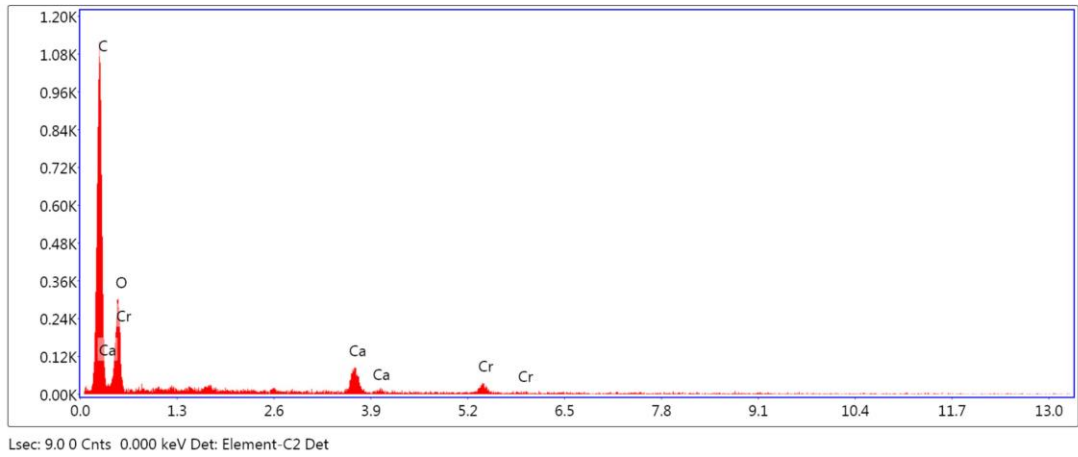


Figure 3.28: EDS spot 2

Table 3.17: eZAF smart quant results of EDS spot 2

Element	Weight %	Atomic %
C K	59.21	67.92
O K	35.21	30.32
CaK	3.51	1.21
CrK	2.06	0.55

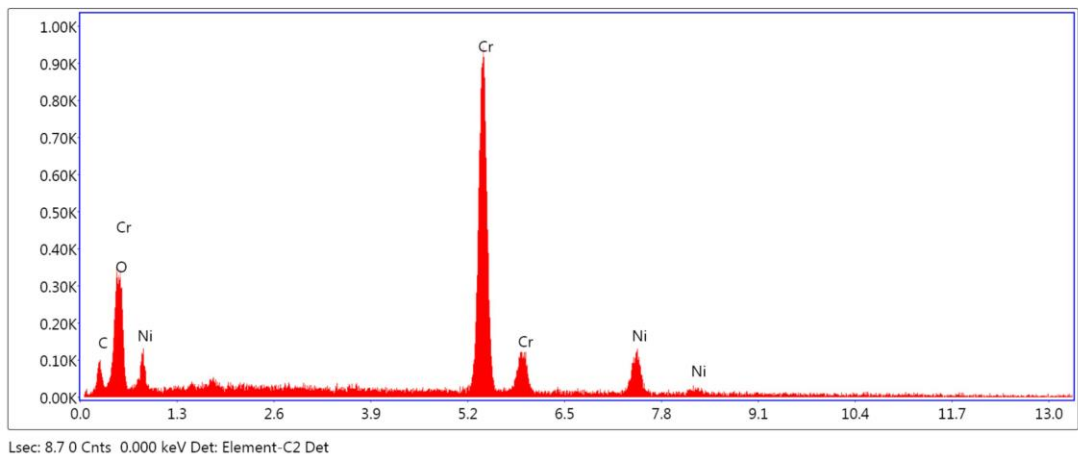


Figure 3.29: Selected area 6



Table 3.18: eZAF smart quant results of area 6

Element	Weight %	Atomic %
C K	6.09	20.89
O K	3.52	9.08
CrK	72.43	57.42
NiK	17.96	12.61

When the oxidation resistance results performed at 1000°C were evaluated, it was observed that there was more weight gain than the test performed at 850°C. When the oxidation resistance results performed at 1000°C were evaluated, it was observed that there was more weight gain than the test performed at 850°C. Looking at the elemental distribution in Figure 3.27, the element carbon in the alloy is the element that interacts the most with oxygen at the closest point to the surface. As seen in Table 3.19, there has been an increase in oxygen and carbon and aluminum element ratios.

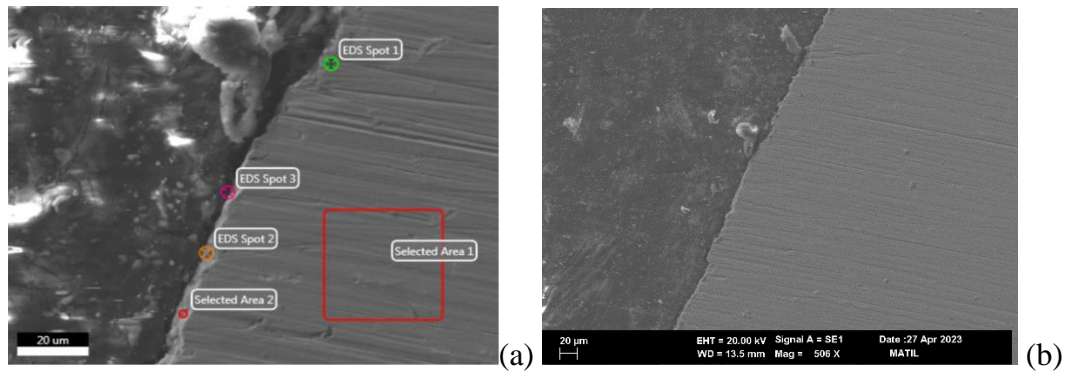


Figure 3.30: Uncoated sample images after 4 cycles of oxidation test at 1000°C

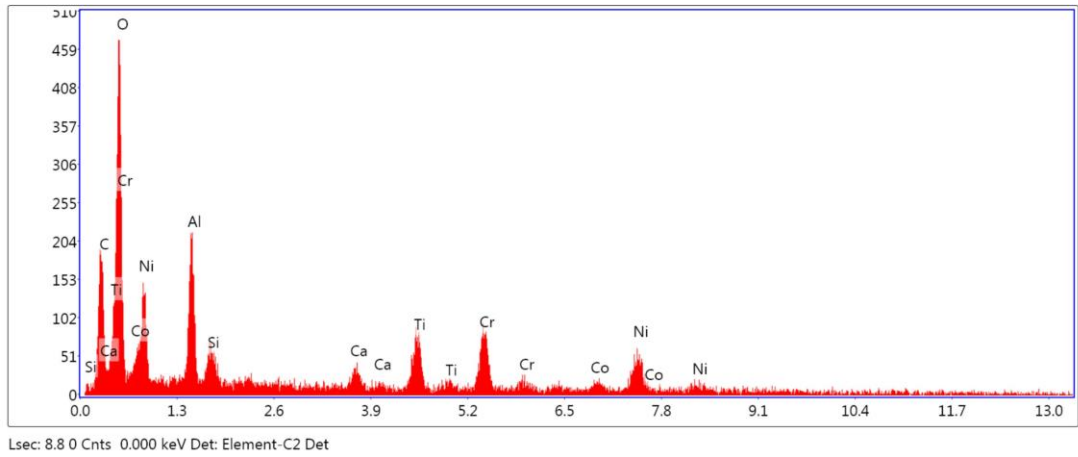


Figure 3.31: Selected area 2

Table 3.19: eZAF smart quant results of area 2

Element	Weight %	Atomic %
C K	23.57	38.40
O K	35.44	43.35
AlK	7.30	5.29
SiK	1.94	1.35
CaK	1.47	0.72
TiK	5.44	2.22
CrK	9.01	3.39
CoK	3.67	1.22
NiK	12.15	4.05

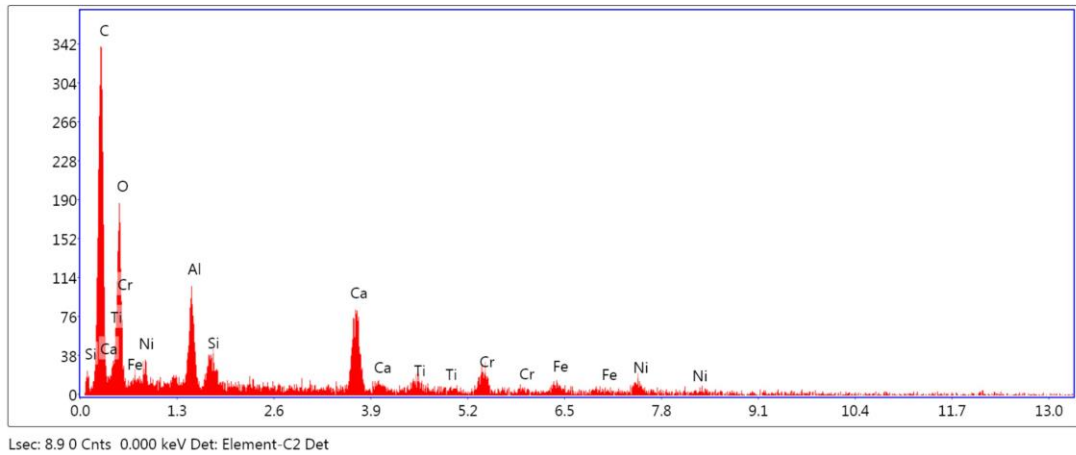


Figure 3.32: EDS spot 3

Table 3.20: eZAF smart quant results of EDS spot 3

Element	Weight %	Atomic %
C K	46.02	61.05
O K	29.59	29.47
AlK	4.02	2.37
SiK	1.54	0.88
CaK	6.69	2.66
TiK	1.83	0.61
CrK	3.57	1.09
FeK	2.56	0.73
NiK	4.18	1.13

Plate-like oxidation separation was observed in (WC-12Co)-33(Cr<sub>2</sub>C<sub>3</sub>-20NiCr) coated samples as seen in Figure 3.33. At the same time, it was observed that pits were formed between the coating and the main material. It is clearly seen that the coating material starts to wear off as a result of oxidation and is detached from the main material surface. Remzi G. et al. stated that tungsten element gains resistance against oxidation with its refractory feature at temperatures of 900°C and above.

Thanks to the oxidation resistance of tungsten, the wear rate of the (WC-12Co)-33(Cr<sub>2</sub>C<sub>3</sub>-20NiCr) coated sample is less than the Cr<sub>2</sub>C<sub>3</sub>-20NiCr coated sample.

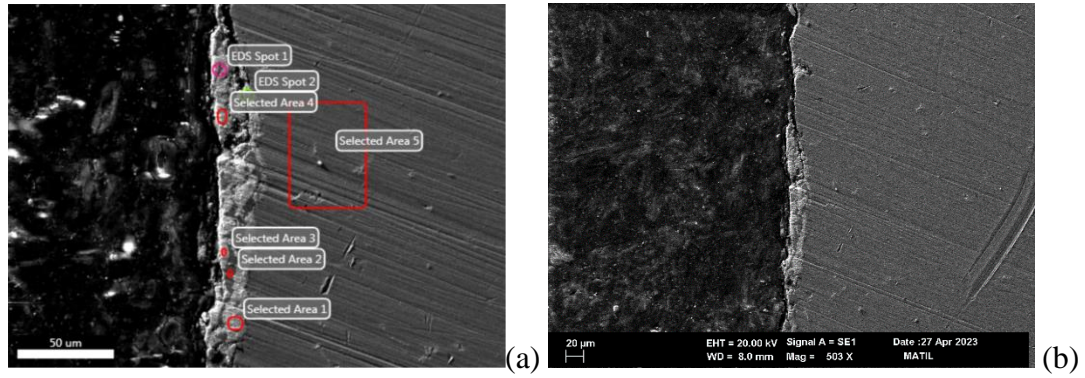


Figure 3.33: (WC-12Co)- 33(Cr<sub>2</sub>C<sub>3</sub>-20NiCr) coated sample images after 4 cycles of oxidation test at 1000°C

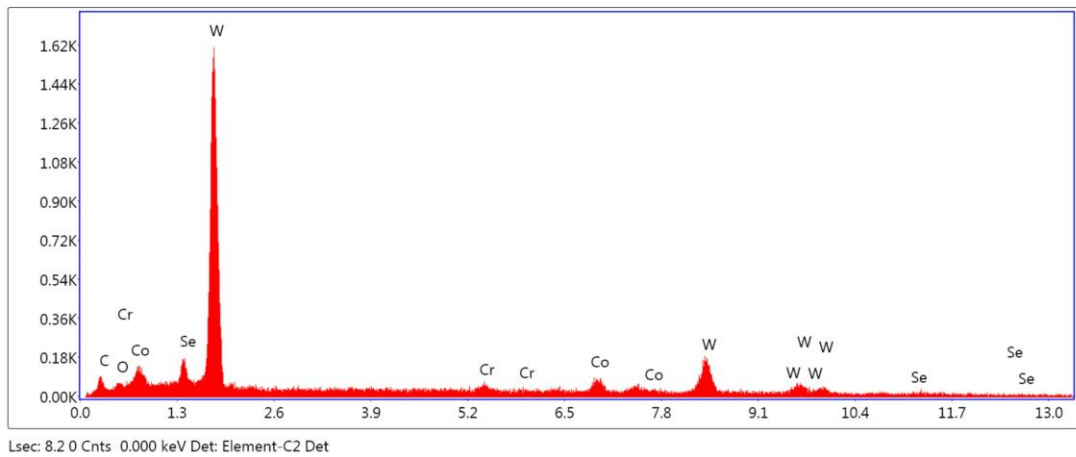


Figure 3.34: Selected area 3

Table 3.21: eZAF smart quant results of area 3

Element	Weight %	Atomic %
C K	3.98	31.11
O K	1.66	9.71
SeL	0.00	0.01
CrK	2.45	4.42
CoK	7.24	11.54
WL	84.66	43.22

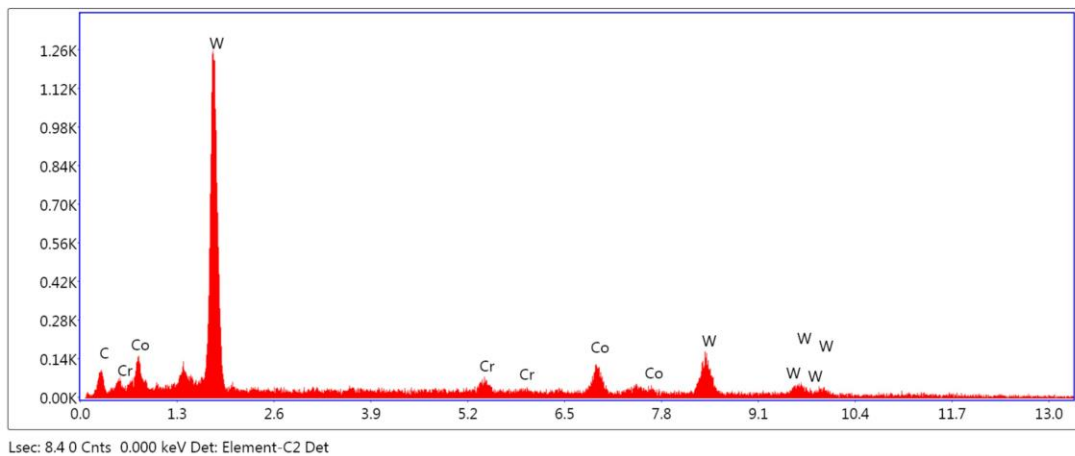


Figure 3.35: EDS spot 2

Table 3.22: eZAF smart quant results of EDS spot 2

Element	Weight %	Atomic %
C K	8.44	50.16
CrK	4.25	5.84
CoK	12.25	14.85
W L	75.06	29.15

In the  $\text{Cr}_2\text{C}_3\text{-20NiCr}$  coated sample, it was observed that capillary cracks formed between the material and the coating due to temperature, as seen in Figure 3.36. Diffusion of chromium from the coating composition and carbon from the sample occurred in the  $\text{Cr}_2\text{C}_3\text{-20NiCr}$  coated sample. It has been observed that the coating is suitable for the sample surface, but as a result of the wear of the coating material due to high temperature, oxygen advances to the sample surface.

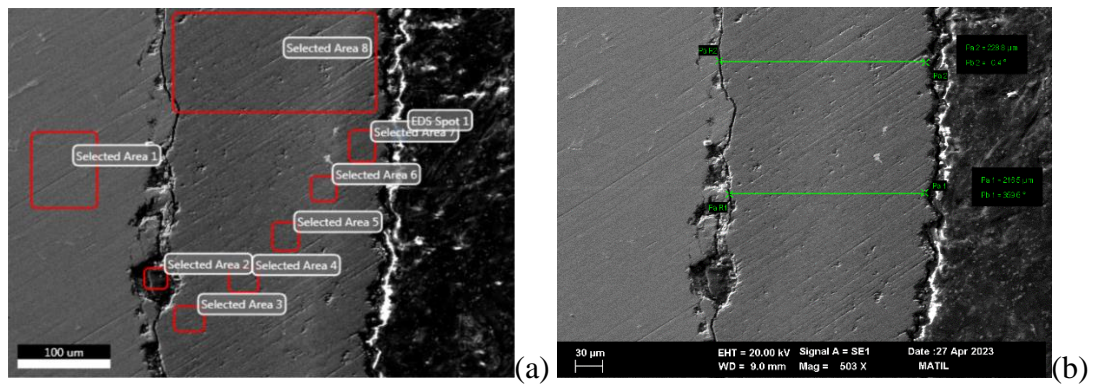


Figure 3.36:  $\text{Cr}_2\text{C}_3\text{-20NiCr}$  coated sample images after 4 cycles of oxidation test at  $1000^\circ\text{C}$

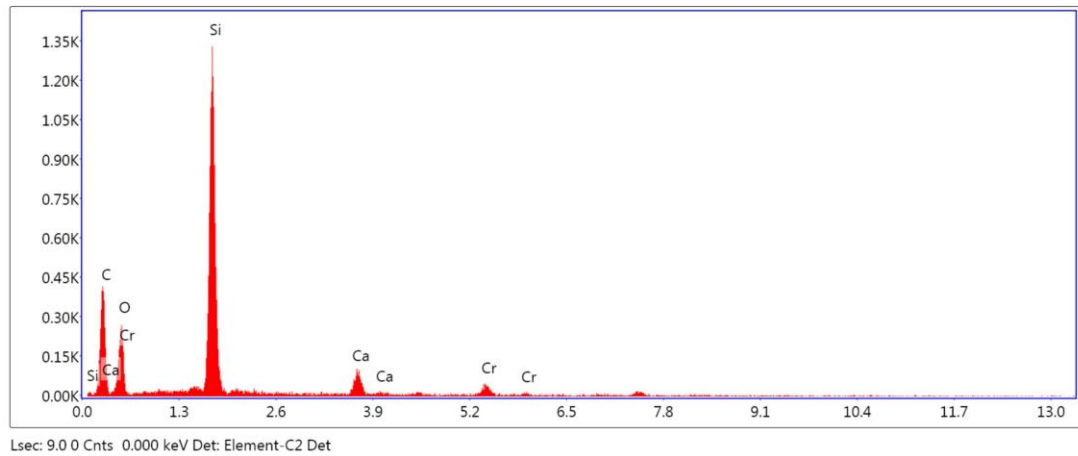


Figure 3.37: Selected area 2

Table 3.23: eZAF smart quant results of area 2

Element	Weight %	Atomic %
C K	47.73	61.84
O K	24.66	23.99
SiK	22.08	12.23
CaK	3.10	1.20
CrK	2.44	0.73

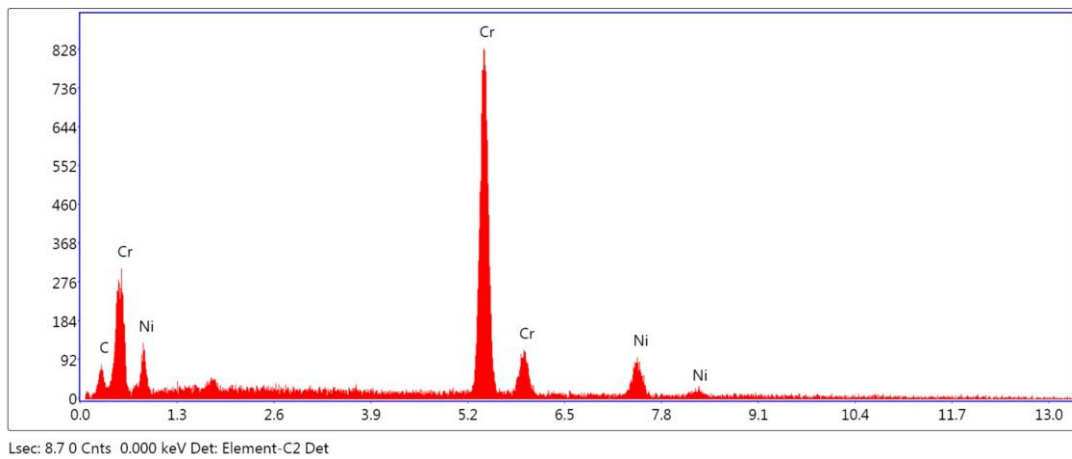


Figure 3.38: Selected area 7

Table 3.24: eZAF smart quant results of area 7

Element	Weight %	Atomic %
C K	5.07	19.08
CrK	78.30	68.10
NiK	16.64	12.81

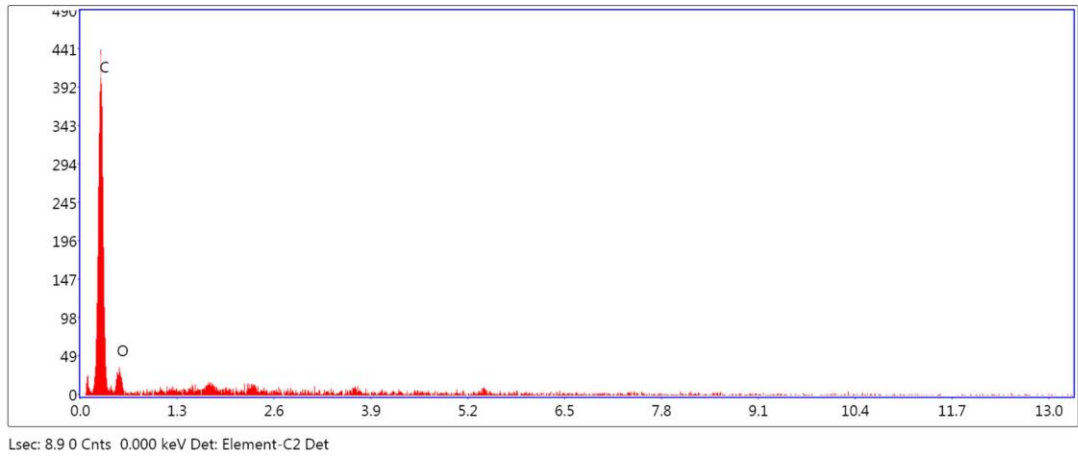


Figure 3.39: EDS spot 1

Table 3.25: eZAF smart quant results of EDS spot 1

Element	Weight %	Atomic %
C K	77.90	82.44
O K	22.10	17.56



# Chapter 4

## Conclusion

- In the first part of the thesis; the effects of carbon element on the mechanical properties of Inconel 738 alloy were investigated.
- As a result of these studies; the positive and negative effects of the carbon element were separated and it was decided that the environmental conditions in the area of use had a significant effect on the choice of carbon ratio. In the stress rupture test results, an increase of 12.7% was observed in the average rupture time with the decrease in carbon content in high temperature environments. However, a decrease of 15.8% (from 16.1% to 13.9%) in the mean elongation value was observed with the decrease of carbon ratio. While the increase in carbon ratio increases the yield and tensile strength of the steel and decreases the percent elongation value, there are situations unlike steel in superalloys. As can be seen from the results, the average percent elongation value increased with higher carbon ratio in Inconel 738 superalloy. With the decrease of carbon ratio, the strength value increased at high temperatures. Although the carbon element has a position as an interstitial atom in the microstructure, it has a positive effect on the elongation value of the material at rupture, although it has reduced the strength. The tensile rupture and tensile test results support this decision.
- In the high temperature tests, an increase of 3.88% was observed in the strength values for both temperatures. It is seen that percent elongation and reduction area percentages of low carbon samples are higher than high carbon samples. It has been clarified that there is no loss in strength in the results of the tensile tests performed at room temperature and 760°C, therefore it can be used in working environments with the temperature where the test is performed. According to the high-temperature

drawing results at 982°C, a 61.17% decrease in strength was recorded with increasing temperature. However, an increase of 81% was observed in the ductility value due to the high temperature at 982°C. Resistance to deformation in hot ambient conditions increased with the decrease of carbon ratio. Carbon addition promotes carbide formation in nickel-based superalloys. While nickel does not form carbide, carbides are formed as a result of the reaction of other alloying elements. The tasks of these formed carbides are complex. The morphology of grain boundary carbides is known to have a detrimental effect on ductility. However, grain boundary carbides also have beneficial effects on general mechanical properties. For example, grain boundary carbides increase tensile strength at high temperatures.

- In the second part; the effect of coating type on high temperature oxidation resistance was investigated. The effects of the elements in the coating alloy and their mixing ratios on the strength were interpreted. When the temperature-dependent behavior of the elements in the oxygen affinity and coating alloys was observed, the oxidation resistances of the tungsten and chromium elements varied depending on the temperatures. Considering the ability of Inconel 738 alloy to work in high temperature environments, it has been observed that the oxidation kinetics are much more successful than the coated samples.
- It has been interpreted that the compatibility between the surface material and the coating material has an effect on the high temperature oxidation resistance.
- When we compared the analyzes of the coated and uncoated samples, it was not seen that the applied coatings provided a positive effect on the oxidation resistance of the Inconel 738 LC material. According to the weight gain results and SEM analysis images, the uncoated sample has less weight loss and less oxide layer and capillary cracks on the surface. In the oxidation test performed at 850°C, the oxygen ratio on the surface was 23% in the uncoated sample, while it increased to 33-36% in the coated samples.
- In the oxidation resistance test performed at 1000°C, although the percent weight gain rate was higher in the Cr<sub>2</sub>C<sub>3</sub>-20NiCr coated sample, it was observed that the coating material was less worn when the line graphs were examined. (WC-12Co)-

$^{33}\text{Cr}_2\text{C}_3\text{-20NiCr}$  coated sample showed a clear decrease in the coating thickness in the line graphs.

# References

- [1] A. Gultekin, "Evolution of Precipitate Microstructure in the Superalloy IN 738 LC During Compression Creep (Master's Thesis)," Boğazici University, 2008, pp. 9, 142-143
- [2] Nisbet, James D., Exploratory High-Temperature Alloy Research, A Design Manual, General Electric Research Laboratory Reports of the Metallurgy Research Department, Part 3, June 1950.
- [3] C.T. Sims, and W. Hagel, (ed.), The Superalloys, Wiley Interscience, New York, 1972.
- [4] Horst Buhl, "Advanced Aerospace Materials", Springer Science and Business Media LLC, 1992
- [5] J.R. Davis, "Superalloys" Asm Technical Books,2001
- [6] Ashby, Michael; Hugh Shercliff; David Cebon, Materials: engineering, science, processing and design (1st ed.). Butterworth-Heinemann, 2007, ISBN 978-0-7506-8391-3.
- [7] H.Coriou, et. al. 'Historical Review of the Principal Research Concerning the Phenomena of Cracking of Nickel Base Austenitic Alloys.' Proceedings of Conference on Fundamental Aspects of Stress Corrosion Cracking and Hydrogen Embrittlement of Iron Base Alloys. Unieux-Firminy France, June 12-16, 1973, NACE-5.
- [8] J.R. Davis, "Superalloys" Asm Technical Books,2001
- [9] S. Lu et al. "Atomic structure and elemental segregation behavior of creep defects in a Co-Al-W-based single crystal superalloys under high temperature and low stress" Acta Mater. (2020)

- [10] Singh, J.B., Introduction. In: Alloy 625 . Materials Horizons, 2022, From Nature to Nanomaterials. Springer, Singapore.
- [11] Andrzej Nowotnik, "Nickel-Based Superalloys" Reference Module in Materials Science and Materials Engineering, 2016
- [12] M.B. Henderson , D. Arrell , M. Heobel, R., "Nickel-Based Superalloy Welding Practices for Industrial Gas Turbine Applications", 2002
- [13] Andrzej Nowotnik, "Nickel-Based Superalloys" Reference Module in Materials Science and Materials Engineering, 2016
- [14] Anil Bhargava, "Heat-Treating Copper and Nickel Alloys", Reference Module in Materials Science and Materials Engineering, 2016
- [15] TaoPeng, BinYang, GangYang, Lu Wang, Zhihu Gong. "Microstructural evolution and mechanical properties of Nimonic 105 alloy aged at 750 °C" Journal of Alloys and Compounds, 2019
- [16] Vedat Veli CAY, Sermin OZAN. "Superalloys And Application Areas" Firat University, Faculty of Technical Education, Department of Metal Education, 2005, ELAZIĞ
- [17] B. C.G. and J. Galka, "Cast Nickel-Base Alloy". United States Patent 3.459.545, 5 August 1969.
- [18] Opeyemi Olorunfemi. "Nickel Based Super Alloys For Gas turbine Applications", University of Ottawa, 2015
- [19] "Alloy In-738 Technical Data" Distributed By Nickel Institute, Inco
- [20] Majid Pouranvari, Aliakbar Ekrami, Amir Hossein Kokabi, "TLP bonding of cast IN718 nickel based superalloy: Process–microstructure–strength characteristics" Materials Science and Engineering, 2013, A 568:76–82

- [21] Nader El-Bagoury, "Ni Based Superalloy: Casting Technology, Metallurgy, Development, Properties And Applications" International Journal Of Engineering Sciences & Research Technology, 2016
- [22] Art Kracke, "Superalloys, The Most Successful Alloy System Of Modern Times - Past, Present And Future ", Vice President Business Technology Ati Allvac, 2010
- [23] Art Kracke, "Superalloys, The Most Successful Alloy System Of Modern Times - Past, Present And Future ", Vice President Business Technology Ati Allvac, 2010
- [24] P.R. Beeley and R.F. Smart. "Investment Casting", The Institute of Materials, 1995, London
- [25] Sachin Thorat, "Steps in Investment Casting Process | Advantages and Disadvantages" in Manufacturing Technology
- [26] Matthew J. Donachie; Stephen J. Donachie, "Superalloys: A Technical Guide (Second Edition), Chapter 8: Heat Treating , Publishing; 2002
- [27] Thomas Publishing Company [Internet], [erişim tarihi 08.12.2022] <https://www.thomasnet.com/articles/chemicals/superalloy-coating-principles/>
- [28] Chellaganesh, D., Adam Khan, M., Winowlin Jappes, J.T., Mashinini, P.M., Surface and Interface Analysis on Plasma Spray Coating on Superalloys at Elevated Temperature. In: Rajkumar, K., Jayamani, E., Ramkumar, P. (eds) Recent Advances in Materials Technologies, 2023, Lecture Notes in Mechanical Engineering. Springer, Singapore.
- [29] Mehdi Abedi-Varaki, Shahram Mollaiy-Berneti. "Modeling of plasma spray coating process using robust solutions based on new intelligence methods" , Universidade Federal de Santa Maria, 2017
- [30] Mathias C. Galetz, "Coatings for Superalloys", Published: November 25th, 2015

- [31] Birks, N.; Meier, Gerald H.; Pettit, F. S., Introduction to the high-temperature oxidation of metals (2nd ed.). Cambridge, UK: Cambridge University Press, 2006
- [32] M. Salehi Doolabi, B. Ghasemi, S.K. Sadrnezhaad, A. Habibollahzadeh, K. Jafarzadeh. "Hot corrosion behavior and nearsurface microstructure of a "low-temperature high-activity Cr-aluminide" coating on Inconel 738LC exposed to Na<sub>2</sub>SO<sub>4</sub>, Na<sub>2</sub>SO<sub>4</sub>+V<sub>2</sub>O<sub>5</sub> and Na<sub>2</sub>SO<sub>4</sub>+V<sub>2</sub>O<sub>5</sub>+NaCl at 900 °C", Corrosion Science, 2017
- [33] Kadir Mert DÖLEKER, Cahit KARAOĞLANLI "The Effect of Cyclic and Isothermal Hot Corrosion on Nickel Based Super Alloy Material", 2020, Volume 7, Issue 2
- [34] O.A. Ojo, Lexie nicole Richards, M. C. Chaturvedi "On incipient melting during high temperature heat treatment of cast Inconel 738 superalloy" Journal of Materials Science, 2004
- [35] Al-Jarba, K.A., Fuchs, G.E. Carbon-containing single-crystal nickel-based superalloys: Segregation behavior and carbide formation. JOM 56, 50–55, 2004.
- [36] L LIU. "Effect of carbon additions on the microstructure in a Ni-base single crystal superalloy", Materials Letters, 2004
- [37] F. S. Pettit and G. H. Meier, "Oxidation And Hot Corrosion Of Superalloys" Pittsburgh, PA 15261, 1984
- [38] Subhash Kamal, R Jayaganthan And S Prakash. "High temperature cyclic oxidation and hot corrosion behaviours of superalloys at 900°C" Bull. Mater. Sci., 2010, Vol. 33, No. 3, June 2010, pp. 299–306. Indian Academy of Sciences. 299
- [39] K. V Sharma, Subhash Kamal, Srinivasa Rao Pedapati, Othman Mamat. "Thermal Spray Coatings for Hot Corrosion Resistance" Engineering Applications of Nanotechnology, 2017, pp. 235-268

- [40] Do Sy, "Material and Application Report 2015 Acrylonitrile Butadiene Styrene (ABS) and 3D Printer (2)" 2015
- [41] PanDaia, "High temperature tensile properties, fracture behaviors and nanoscale precipitate variation of an Al–Zn–Mg–Cu alloy" Progress in Natural Science: Materials International, 2020
- [42] Jyri Outinen, "Mechanical Properties of Structural Steels at High Temperatures and After Cooling Down" Helsinki University of Technology Laboratory of Steel Structures Publications 32, 2007
- [43] Laboratory Testing Inc. [İnternet], [erişim tarihi 15.12.2022]  
<https://labtesting.com/services/materials-testing/mechanical-testing/stress-rupture/>
- [44] EXTRUDESIGN.COM [İnternet], [erişim tarihi 15.12.2022]  
<https://extrudesign.com/what-is-creep-and-stress-rupture-of-metals/>
- [45] KBT BİLİM SİTESİ [ İnternet ], [erişim tarihi 18.12.2022]  
<https://www.kuark.org/2017/04/taramali-elektron-mikroskobu-sem-eds-analizi/>
- [46] Vedat Veli ÇAY, “Superalloys and Application Areas” Firat University Technical Education Faculty Metal Education Department, ELAZIG, 2005



# Curriculum Vitae

Name Surname: Simge AVCI

Education:

2014-2020 İzmir Katip Celebi University, Department of Material Science and Engineering

Internships:

2017- CMS Jant ve Makine San. A.ş. (Production and Quality)

2018- VOESTALPINE High Performance Metals USA (Sales and Quality)

Experience:

2020 Varzene Metal San ve Tic. A.Ş (Quality Assurance Manager)